Effect of Waste Settlement and Seismic Loading on the Integrity of Geomembrane Barrier Systems

by

Xuan Wu

A Thesis Presented in Partial Fulfillment
of the Requirements for the Degree
Master of Science

Approved November 2013 by the
Graduate Supervisory Committee:

Edward Kavazanjian
Claudia Zapata
Sandra Houston

ARIZONA STATE UNIVERSITY

November 2013

ABSTRACT

The objective of the research is to develop guidelines for identifying when settlement or seismic loading presents a threat to the integrity of geosynthetic elements for both side slope and cover systems in landfills, and advance further investigation for parameters which influence the strains in the barrier systems.

A numerical model of landfill with different side slope inclinations are developed by the two-dimensional explicit finite difference program FLAC 7.0, beam elements with a hyperbolic stress-strain relationship, zero moment of inertia, and interface elements on both sides were used to model the geosynthetic barrier systems. The resulting numerical model demonstrates the load-displacement behavior of geosynthetic interfaces, including whole liner systems and dynamic shear response. It is also through the different results in strains from the influences of slope angle and interface friction of geosynthetic liners to develop implications for engineering practice and recommendations for static and seismic design of waste containment systems.

DEDICATION

This thesis is dedicated to my Mother and Father who have supported me all the way since the beginning of my studies.

ACKNOWLEDGMENTS

The time I have spent at Arizona State University has been a rewarding experience both academically and personally. I want to thank all my colleagues and friends that made these years a joyful and beneficial time.

I would like to thank my advisor Professor Edward Kavazanjian, Jr. for his invaluable guidance during the course of my studies. I am grateful that he provided the encouragement and patience that I needed.

TABLE OF CONTENTS

Page

LIST OF TABLES

Table Page

LIST OF FIGURES

Figure Page

CHAPTER 1 INTRODUCTION

1.1 OBJECTIVE

The objective of this dissertation is to study the combined impacts of large settlement and seismic loading on the integrity of the geosynthetic elements of municipal solid waste (MSW) landfill liner and cover systems. Integrity is assessed by evaluating the forces and strains induced by these extreme loading events on the geosynthetic elements of the containment system. The mechanical behavior of the geosynthetic elements of engineered waste containment barrier systems subject to extreme loads, e.g. large settlement or seismic loading, is an important problem in geoenvironmental engineering. The induced forces and strains which threaten the integrity of geomembrane (GM) and geosynthetic clay liner (GCL) barrier layers and geosynthetic drainage layers are typically not explicitly evaluated in design but should not be ignored in design of waste containment barrier systems.

1.2 BACKGROUND

Geosynthetic materials are often vulnerable to tensile strains induced by external loading. Current landfill design practice does not explicitly consider the development of tension in the containment system elements, despite analyses and field observations indicating that tensile forces induced by seismic loading can exceed the tensile strength of these materials (Anderson and Kavazanjian 1995; Augello et al. 1995; EMCON

Associates 1994). The large settlement of MSW landfill waste can also drag down and induce tensile strains on the GM and GCL elements of the side slope liner system. Excessive tensile strains can potentially cause irreparable damage to the geosynthetic elements of a landfill liner system. Furthermore, the damage due to tensile strains induced by settlement or seismic loading may be hidden beneath the waste, with no surface expression to these systems to alert the engineer, operator, owner, or regulator that there is a problem.

Geosynthetic barrier systems have been mandated for MSW landfill liner and final cover systems in the United States for almost 20 years. The typical geosynthetic elements employed in landfill liner and cover systems include GMs, GCLs, and geosynthetic drainage layers. Geomembranes have been explicitly included in the prescriptive liner and implicitly included in the cover system for MSW landfills with geosynthetic liners under Subtitle D of Title 40 of the Code of Federal Regulations (40 CFR) since 1993. The prescriptive liner system in Section 258 of the 1993 Subtitle D regulations (40 CFR 258) calls for a GM at least 40 mil (1 mm) in thickness, and 60-mil (1.5 mm) thick if high density polyethylene (HDPE) is used, overlying a compacted clay liner (CCL) in the basal liner system. These regulations also require that landfills should be capped with a cover system that has a lower permeability than the liner, a requirement widely interpreted as implicitly requiring a geomembrane in the cover if a geomembrane is

employed in the liner. Subtitle D also requires that MSW landfills in approximately 40% of the continental United States must be designed for seismic loading.

GCLs and geosynthetic drainage layers are discretionary alternatives to compacted low permeability soil layers and granular soil drainage layers, respectively, in MSW landfill liner and cover systems. GCLs are 6 mm-thick layers of powdered or granulated sodium bentonite bound by a water soluble glue and either sewn or needle-punched between two geotextiles or adhered to a geomembrane. GCLs are frequently preferred as alternatives to compacted low permeability soil layers for side slope liner systems in quarry and canyon landfills, where steep slopes make construction of a CCL difficult and expensive. GCLs also provide the cost-effective benefits with respect to ease of construction and quality assurance, provide increased useable airspace, and offer reduced environmental impacts (less dust, less noise, less vehicle emissions, lower water use) during construction (Fox and Stark 2004). Geosynthetic drainage layers (a plastic drainage core protected by a filter geotextile) are also often preferred for side slope liner systems, as the gradient of the side slope often makes placement of granular drainage layers difficult, if not impossible, and also offer cost advantages over granular drainage layers in many cases.

The forces and strains induced on the elements of MSW landfill liner and cover systems by large waste settlement under static loading have been shown by Dixon and his co-workers (Dixon and Jones 2005, Fowmes at al. 2005) to be of concern with respect to

the integrity of geosynthetic barrier systems in landfills. Municipal solid waste (MSW) is subject to significant volume change after placement in a landfill due to decomposition and high compressibility. This compression produces large settlements during filling operations and after closure (Edil et al. 1990, El Fadel et al. 1999, Park et al. 2002). A MSW landfill will sometimes settle on the order of 20% of the overall waste thickness after the end of waste placement. These settlements may induce large shear forces in the liner system along the side slopes of the landfill and may also cause potential problems with the integrity of the cover system. Large shear forces on the side slopes of the landfill may produce tensile strains large enough to damage the geosynthetic components of the liner system. Fowmes et al. (2005) analyzed the behavior of a typical quarry landfill liner system in the U.K. using the computer program FLAC^{TM} and demonstrated that waste settlement can cause excessive tensile strain in the geosynthetic elements of the liner on the side slope. Figure 1-1 shows typical mechanisms for failure of side slope liner systems due to the large waste settlement identified by Dixon and Jones (2005), including damage to the geosynthetic elements of the liner system.

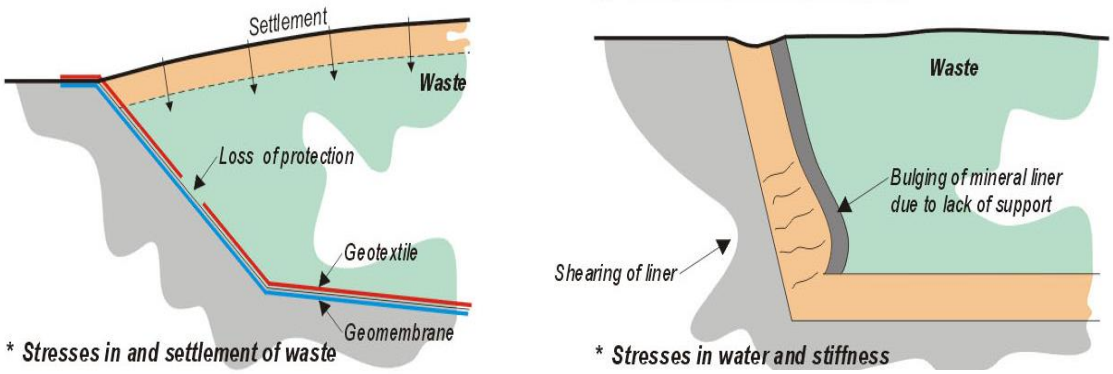

Figure 1-1. Mechanisms of local side slope integrity failure (Dixon and Jones 2005)

Seismically-induced tensile forces and strains also have the potential for inducing tensile strains that can impair the integrity of geomembrane (GM) and geosynthetic clay liner (GCL) barrier layers and other geosynthetic elements of the containment system. Tears observed in the geomembrane side slope liner at the Chiquita Canyon landfill following the 1994 Northridge earthquake in southern California (EMCON 1994) graphically illustrate the potential for seismically induced damage to a side slope liner system. Figure 2 shows the tears it the crest of the slope in the Canyon C landfill unit at Chiquita Canyon observed following the Northridge earthquake.

Arab (2011) developed a large-strain finite difference FLAC^{TM} numerical model for predicting the in plane shear behavior of the geosynthetic elements of a liner system under both static and seismic loading. Back-analyses of the performance of the liner system at Chiquita Canyon during the Northridge earthquake conducted by Arab (2011) using this model demonstrated that the tensile strains in the GM at the crest of the slope

exceeded allowable values once geomembrane strain concentrations were taken into account. These Arab (2011) analysis demonstrated the potential for the forces and strains induced by seismic loading to damage side slope liner systems, but neither the combined effect of waste settlement and seismic loading on liner and cover systems were considered by Arab (2011).

Figure 1-2. Tear in geomembrane liner system, Cell C, Chiquita Canyon Landfill after 1994 Northridge earthquake (photo courtesy of Calif. EPA, Integrated Waste Management Board)

The objective of the research described in this dissertation is to develop guidance for identifying when settlement or seismic loading presents a threat to the integrity of geosynthetic elements for both side slope liner and cover systems in landfills. The work includes parametric investigation of the parameters which influence the tensile strain induced the elements of the barrier systems of liners and covers. A numerical model of a "typical" MSW landfill with different side slope inclinations is developed following the methodology developed by Arab (2011), i.e. using the two-dimensional explicit finite difference program FLAC^{TM} and employing beam elements with a hyperbolic stress-strain relationship, zero moment of inertia, and interface elements on both sides to model the geosynthetic barrier system elements. The analyses conducted using this numerical model demonstrate the importance of interface shear strength on load-displacement behavior and the induced tensile strains and forces in side slope liner systems. The analyses also demonstrate the influence of slope angle on the strains and forces induced in geosynthetic liner system elements and provide a basis from which to develop recommendations for static and seismic design of waste containment systems.

1.3 ORGANIZATION OF THIS THESIS

This dissertation is organized as follows:

- Chapter 2 presents a review of background literature essential to the analyses conducted in this thesis. The engineering characteristics of the various components of landfill (e.g. solid waste, geosynthetic lining material) are

discussed along with the large strain finite difference numerical model developed by Arab (2011) using FLAC^{TM} 7.0 (Itasca 2008) for evaluating the strains and forces in the geosynthetic components of the landfill.

- Chapter 3 presents the characteristics of Cam-Clay model used to represent MSW in FLAC 7.0 (Itasca 2008). The properties of this model required to induce a post-placement waste settlement equal to 20 percent to the waste thickness at the completion of waste placement are established in this chapter.
- Chapter 4 presents a numerical model of a typical MSW landfill with relatively steep side slopes (3H:1V, horizontal:vertical, or steeper) . This model is sued to evaluate the impact of waste settlement on the tensile forces and strains in geosynthetic elements of the liner system. Various parameters which influence the strains in the geosynthetic liner and cover systems are investigated in this chapter.
- Chapter 5 presents the results of analyses of the combined impact of settlement and seismic loading on the tensile forces and strains induced in geosynthetic elements of the containment system for the typical cross section established in Chapter 4. The analyses are performed using the ground motion records from the Northridge earthquake. This chapter includes sensitivity analyses conducted to investigate the influence of various model parameters on the tensile stresses and forces in the geosynthetic elements of the model.

- Chapter 6 contains the summary and conclusions draw from this study, including the implications for engineering practice and recommendations for future research and development.

CHAPTER 2 BACKGROUND INFORMATION

2.1 INTRODUCTION

This chapter will review available information on the settlement of MSW, the mechanical behavior of typical geosynthetic elements of waste containment systems, and numerical analysis of the performance of geosynthetic elements of waste containment systems.Municipal solid waste (MSW) generally refers to common household waste, as well as office and retail wastes, but excludes industrial, hazardous, and construction wastes. The cyclic and static mechanical properties of MSW are significant with respect to accurate static and/or seismic analyses of landfill containment system elements. In particular, the characteristic of large waste settlement is an important factor affecting the axial force induced by service loads in geosynthetic barrier systems. In addition, the internal and interface behavior of geosynthetics under shear stress also play a crucial role in the assessment of the dynamic and static performance of landfills systems.

2.2 MSW LANDFILL SETTLEMENT

Due to its compressible nature and to decomposition after waste placement, MSW landfills suffer from large settlement both during waste placement and over an extended period of time after the end of waste placement. Decomposition after the end of waste placement may induce settlement as large as 30%-40% of the initial fill height, although 20% is often quoted as a typical value. The large settlement associated with MSW

landfilling may induce tensile loads in liner system elements and, in the post-closure period, may also lead to surface ponding and development of cracks in soil layers in the cover system. Therefore, studies on the characteristics of waste settlement are an important element in the analysis and design of geosynthetic barrier systems.

Ling et al. (1998) conducted a detailed study of post-closure landfill settlement. Three case studies of settlement or settlement rate were used to examine the accuracy of several different empirical models. These models quantified the relationship between the settlement (or settlement rate) and time by two types of functions: a power function and a hyperbolic function.

The power function proposed by Edil et al. (1990) and presented below as equation 2-1 was used by Ling et al. (1998) to relate settlement rate with time:

$$\rho = \frac{dS}{dt} = \frac{p}{t^q} \tag{2-1}$$

where p and q are positive empirical constants. In Eq. 2-1, p is the settlement rate at unit time. An equation for settlement may be developed by integrating Eq. 2-1, yielding Eq. 2-2:

$$S = p' \cdot t^{q'} \tag{2-2}$$

Alternatively, settlement can expressed directly using the traditional secondary compression equation as a function of log t:

$$S = m' + n' \cdot \log t \tag{2-3}$$

where m', n', p' and q' are positive empirical constants. Note that p' may be considered as the settlement at unit time.

A hyperbolic function relating settlement and time can be expressed follows:

$$S = \frac{t}{1/\rho_0 + t/S_{ult}} \tag{2-4}$$

where t is the difference between the time of interest and the start of settlement measurement; S is the settlement over time t; ρ_0 is the initial rate of settlement; and S_{ult} represents the ultimate settlement.

Measurements of post-closure settlement versus time were analyzed for three landfills: a Southeastern Wisconsin landfill (Edil et al. 1991); the Meruelo landfill in Spain (Sanchez-Alciturri et al. 1995); and the Spadra landfill in southern California (Merz and Stone 1962). Figure 2-1 shows the settlement data fitted to the S-log t and power functions. In fitting the data to the power function, some of the initial data was excluded to obtain satisfactory agreement for long-term settlement.

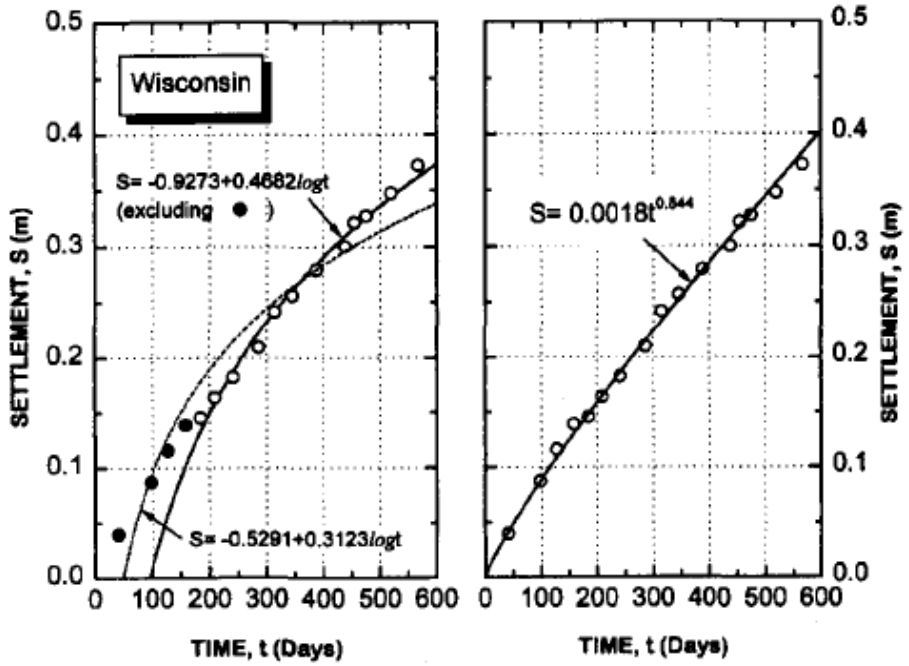
Wisconsin
S= -0.9273+0.4682logt
(excluding ●)
S= -0.5291+0.3123logt
S= 0.0018t^0.844
SETTLEMENT, S (m)
TIME, t (Days)
0.0
0.1
0.2
0.3
0.4
0.5
0 100 200 300 400 500 600

(a)

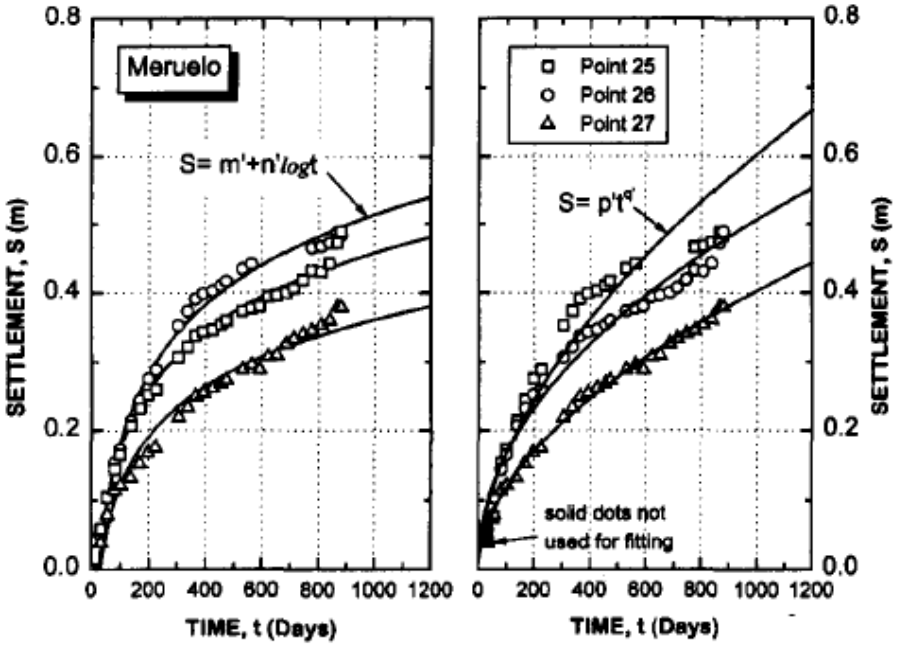
Meruelo
S= m'+n'logt
S= p't^q'
Point 25
Point 26
Point 27
solid dots not
used for fitting
SETTLEMENT, S (m)
TIME, t (Days)
0.0
0.2
0.4
0.6
0.8
0 200 400 600 800 1000 1200

(b)

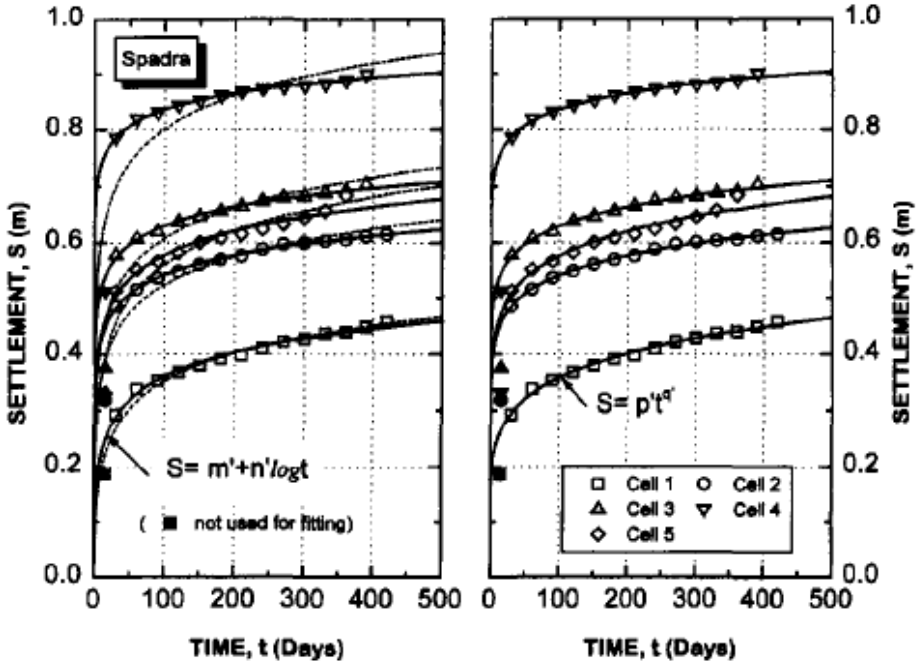

(c)

Figure 2-1. Settlement estimation based on S-log t and power functions: (a) SE Wisconsin landfill; (b) Meruelo landfill; (c) Spadra landfill (Ling et al. 1998)

The use of a hyperbolic function to fit the data is illustrated in Figure 2-2. Using the best fit curve, the average ultimate settlement, S_{ult}, for the three landfills were determined as 1.14m, 0.57m, and 0.69m for the Wisconsin, Spain, and California landfills, respectively.

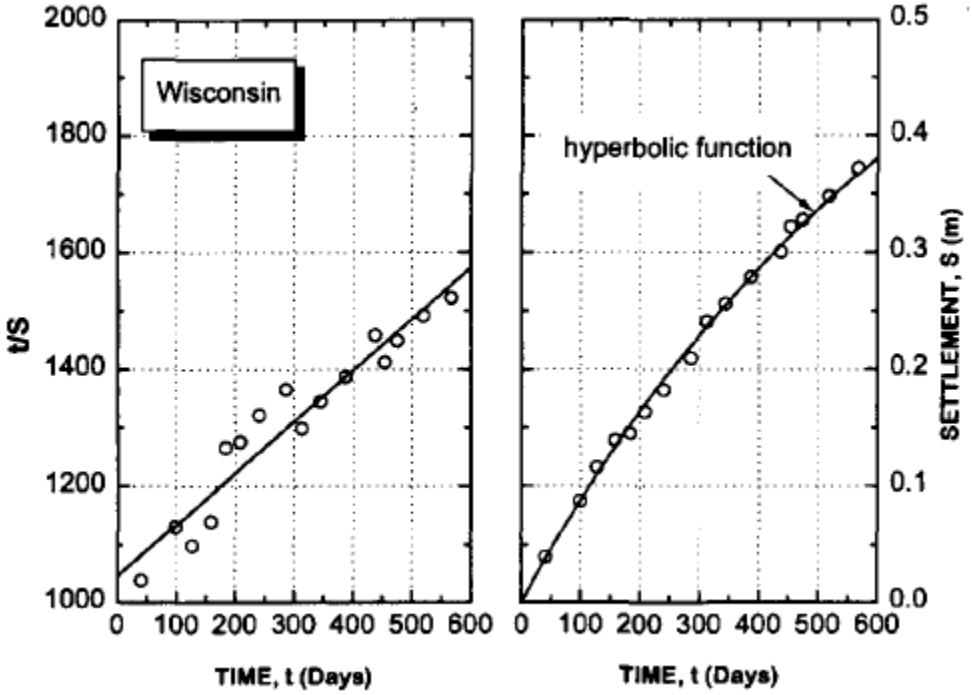
Wisconsin
hyperbolic function
t/S
SETTLEMENT, S (m)
TIME, t (Days)
TIME, t (Days)
2000
1800
1600
1400
1200
1000
0.5
0.4
0.3
0.2
0.1
0.0
0 100 200 300 400 500 600

(a)

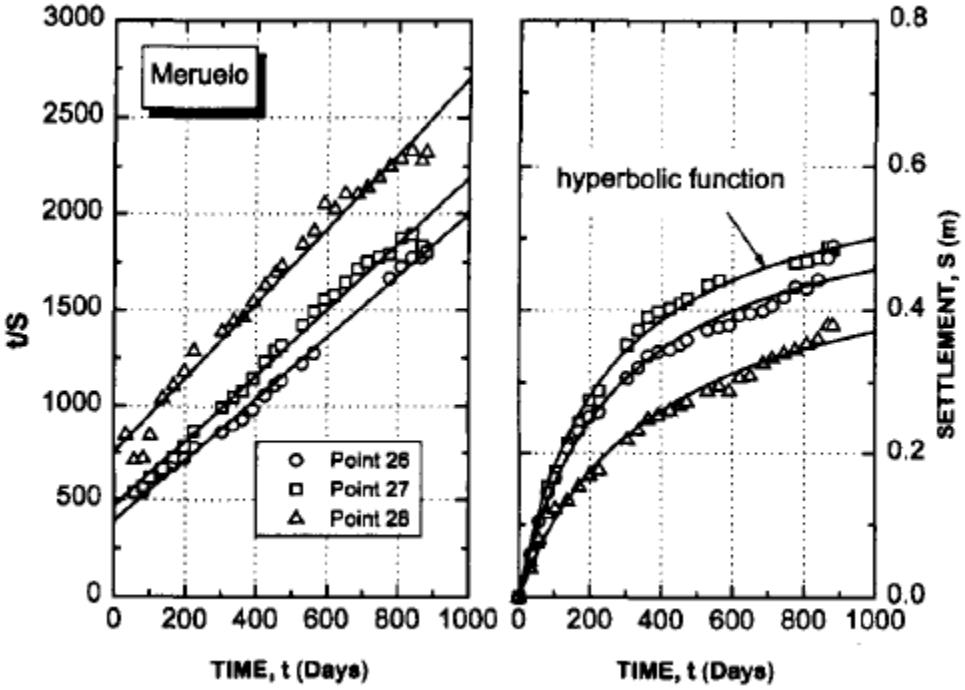
Meruelo
hyperbolic function
Point 26
Point 27
Point 28
t/S
SETTLEMENT, S (m)
TIME, t (Days)
TIME, t (Days)
3000
2500
2000
1500
1000
500
0
0.8
0.6
0.4
0.2
0.0
0 200 400 600 800 1000

(b)

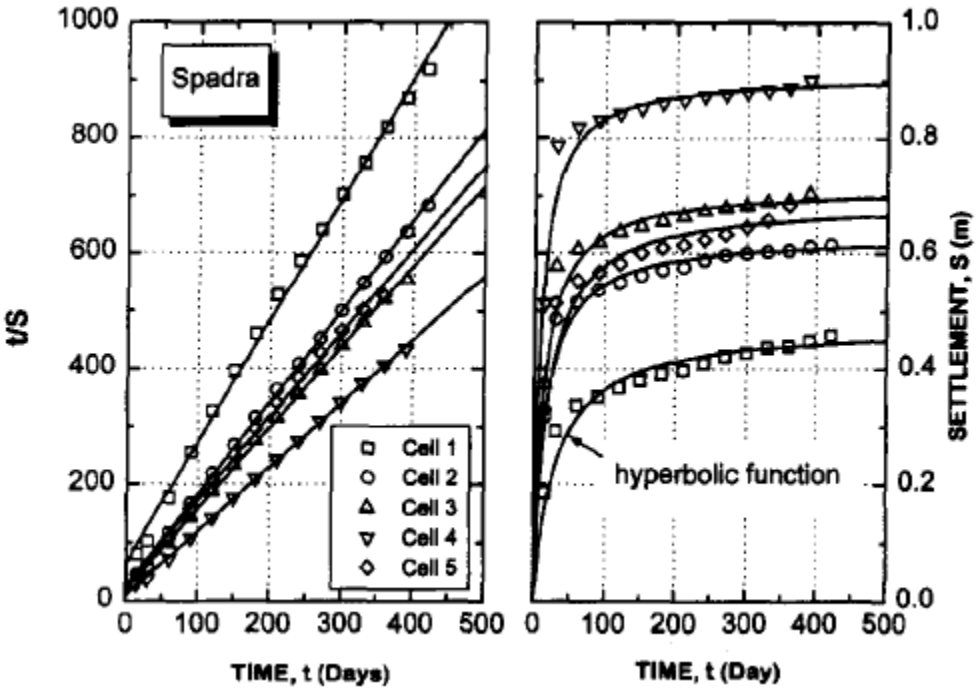

Figure 2-2. Settlement estimation based on hyperbolic functions: (a) SE Wisconsin landfill; (b) Meruelo landfill; (c) Spadra landfill (Ling et al. 1998)

Post-closure settlement of a MSW landfill are typically assumed be on the order of 20% of the waste thickness (personal communication, Professor Edward Kavazanjian).

2.3 NUMERICAL MODELLING OF MULTILAYERED GEOSYNTHETIC LANDFILL LINING SYSTEMS

Dixon and Fowmes (2007) developed a method for numerical modeling of the performance of the geosynthetic elements of a multilayered lining system in a landfill subject to downdrag forces from settlement of a compressible waste material. The tensile

stresses in the geosynthetics and relative displacements at interfaces were predicted using the computer program FLAC^{TM}. The results from their numerical analysis were compared to the data from a series of large scale laboratory tests.

2.3.1 Laboratory Testing

Large scale laboratory tests were employed by Dixon and Fowmes (2007) to represent the interaction of geosynthetic lining system components with landfill waste when exposed to downdrag forces. These tests were designed to generate post-peak interface displacements similar to those that may be experienced in landfill side slope lining systems. The testing configuration is shown in Figure 2-3 (Dixon and Fowmes 2007). A compressible synthetic waste was placed in an open box which had a sacrificial slip surface in one side and a multiple geosynthetic layer lining system on the other side. Waste settlement was induced by a vertical load supplied from a hydraulic jack on top of the waste. A displacement gauge recorded the settlement of waste and the relative displacements at different interfaces of the multi-layer geosynthetic lining system were recorded using wire displacement gauges. Interface behavior was evaluated for three types of geosynthetic interfaces: wood – geomembrane; geomembrane – geotextile; and geotextile – synthetic waste. Geomembranes from three different manufacturers were used in the tests. Table 2-1 lists the properties of the three geomembranes used in the tests. The peak and large displacement adhesion, α, and friction angle, δ, of the various interfaces are summarized in Table 2-2.

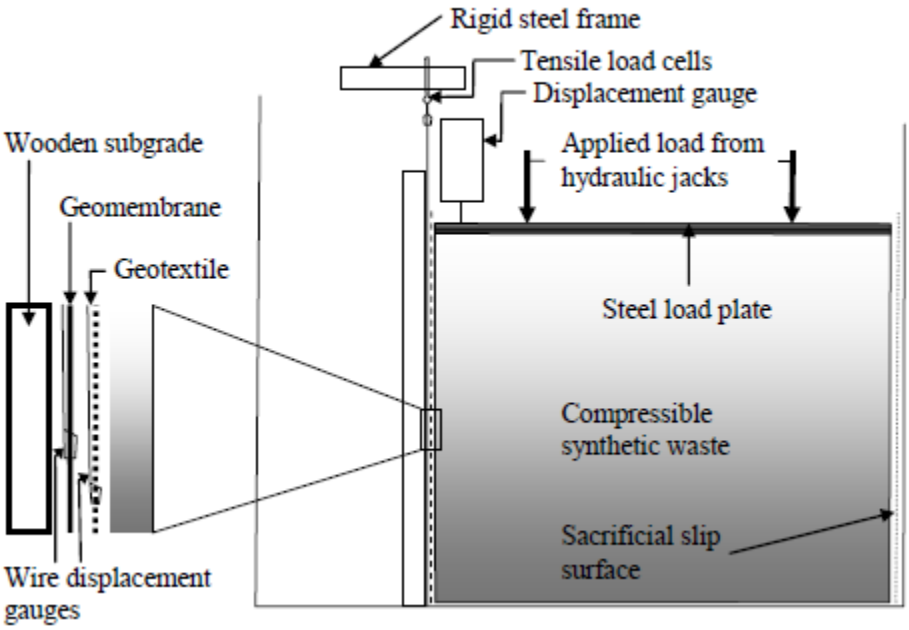

Figure 2-3. Schematic of measuring box (Dixon and Fowmes 2007)

Table 2-1 Geomembrane Properties (Dixon and Fowmes 2007)

	Type G LLDPE	Type S LLDPE	Type G HDPE
Polymer Type	LLDPE	LLDPE	HDPE
Manufacturer	G	S	G
Texturing	Double	Double	Mono
Texturing Type	Impinged	Blown film	Impinged
2% modulus	$4.2x10^5$ kPa	$4x10^5$ kPa	$7x10^5$ kPa
Compressive modulus (assumed)	$4.2x10^4$ kPa	$4x10^4$ kPa	$7x10^4$ kPa
Thickness	1 mm	1 mm	1 mm
Yield strength			16 kN/m
Yield Elongation			9%
Break Strength	12 kN/m	17.5 kN/m	10 kN/m
Break Elongation	250%	400%	100%

Table 2-2 Summary of peak interface shear strengths (Dixon and Fowmes 2007)

Interface	α_{peak} (kPa)	δ_{peak} (°)	α_{LD} (kPa)	δ_{LD} (°)	Test
Synthetic Waste vs. Geotextile	4.4	29.9	3.3	29.8	All
Type G LLDPE GM vs. Geotextile	8.2	27.5	5.6	16.5	T2 & T5
Type G LLDPE GM vs. Wood	1.0	8.9	0.5	8.1	
Type S LLDPE GM vs. Geotextile	1.0	29.0	2.0	18.8	T6 & T9
Type S LLDPE GM vs. Wood	0.7	9.8	0.8	7.7	
Type G HDPE (tex) GM vs. Geotextile	8.0	29.4	5.4	18.7	T3
Type G HDPE (smooth) GM vs. Wood	0.8	10.1	0.5	10.2	
Type G HDPE (smooth) GM vs. Geotextile	0.4	11.7	0.4	9.0	T4
Type G HDPE (tex) GM vs. Wood	0.8	9.2	0.4	8.0	

2.3.2 Numerical Modeling

The large strain finite difference numerical modeling program FLAC 4.0 (Fast Lagrangian Analysis of Continua Version 4.0) was employed by Dixon and his co-workers (Dixon and Fowmes 2008; Fowmes at al. 2005, 2006) to analyze side slope lining systems subject to downdrag primarily due to its ability to model large strains. A later version of FLAC, Version 7.0, was employed by Arab (2011) to model the impact of seismic loading on the integrity of the geosynthetic elements of landfill liner systems.

FLAC is a two-dimensional explicit finite difference program designed specifically to model the behavior of structures built of soil, rock or other continuum materials that may undergo plastic flow when their yield limits are reached in response to applied forces and boundary restraints. Continuum materials are represented by elements, or zones, which form a grid that is adjusted by the user to fit the shape of the object to be modeled.

Each element behaves according to a prescribed constitutive model. In addition to the constitutive models built in FLAC, user defined constitutive models can be employed. The material within an element can yield and flow and the grid deforms (in large-strain mode) according to the movement of the material within it. An explicit Lagrangian calculation scheme and the mixed-discretization zoning technique is used in FLAC to ensure that plastic collapse and flow are numerically stable and modeled accurately.

In the numerical analysis of laboratory interface shear tests conducted by Dixon and Fowmes (2008), they modeled the behavior of the waste using a linear elastic material model with a Mohr-Coulomb failure criterion. They assigned a shear strength to the waste characterized by a 29.3° friction angle and 3 kPa of cohesion. The geosynthetic elements were modeled as structural beam elements with zero moment of inertia (following Itasca 2002). Multiple beam elements were placed in the nulled region between two grid elements to model the multiple layers of geosynthetic materials. One grid element represented the synthetic waste and the other grid represented the subgrade. The beams interacted with each other and with the grid through interface elements. The interface elements were assigned normal and shear stiffness and shear strength parameters intended to represent their shear and normal displacement characteristics. Prior to applying a load to the top of the waste grids, each waste zone (or element) had a height of 20 mm. The load was applied by applying a vertical stress to the upper surface

of the waste material grid. Figure 2-4 shows the FLAC grid geometry used by Dixon and Fowmes (2008) to model their laboratory interface shear tests.

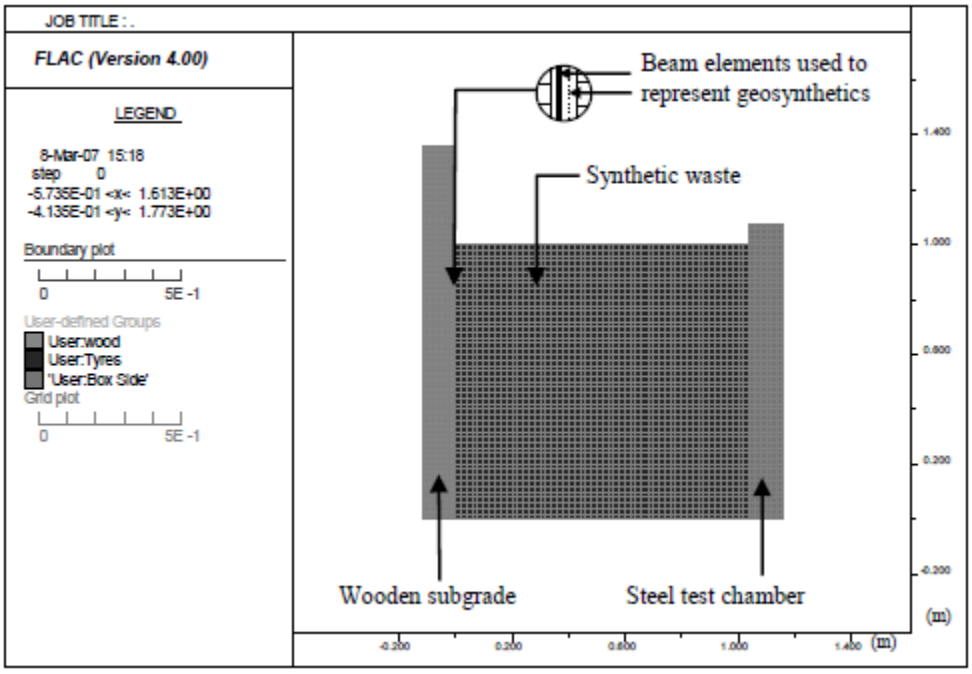

Figure 2-4. FLAC grid 20 mm grid zones (prior to deformation) used to model laboratory shear tests (Dixon and Fowmes 2008)

2.3.3 Results of the numerical analysis of laboratory interface shear tests

Good agreement was obtained by Fowmes and Dixon (2007) in many cases between the measurements made in the laboratory tests and the results of the numerical analyses using FLAC. However, in some cases discrepancies were observed. Figure 2-5 presents comparisons between the measured and modeled tension at the geomembrane anchorage for the model tests described in Tables 2-1 and 2-2.

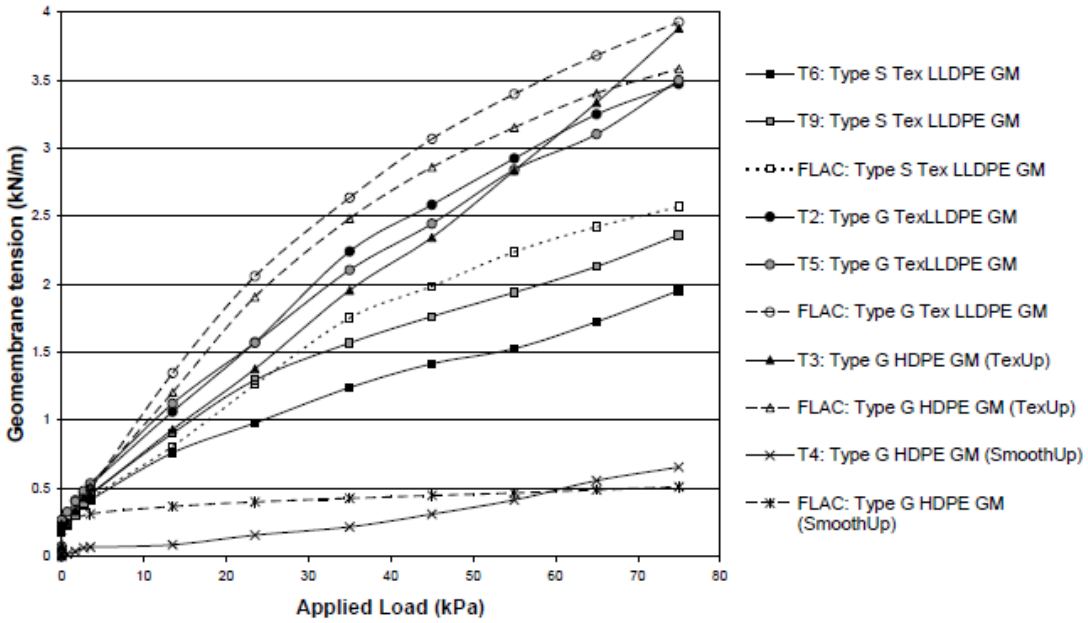

Figure 2-5. Tension in the geomembrane, at anchorage, from laboratory tests and FLAC models (Fowmes and Dixon, 2007)

Dixon and Fowmes (2007) attributed the discrepancies between the numerical analysis values and the measured behavior to simplifications in modeling geosynthetic axial stress response (in both tension and compression) and with the constitutive model used to represent the synthetic waste (which was crumb rubber). However, they concluded that the FLAC model was an appropriate way to model the performance of geosynthetic liner systems. Dixon and Fowmes (2007) also concluded that the numerical modeling accuracy is limited by the accuracy of the input parameters.

Fowmes and Dixon (2005) also directly modeled side slope liner performance of a prototype landfill. Figure 2-6 shows the structure of the slope liner system employed in their research. A benched quarry side slope with a geosynthetic lining system from a

large landfill in South East Asia was represented by the two FLAC models shown in Figure 2-7. The first model was a full height section of side slope and was used to assess the waste and lining system behavior on a multiple bench quarry subgrade. The second model was a detailed model of a single section of the side slope and was employed to assess the behavior of the lining system in more detail over a single bench height. The interface and geosynthetic properties employed in these analyses are shown in Table 2-3.

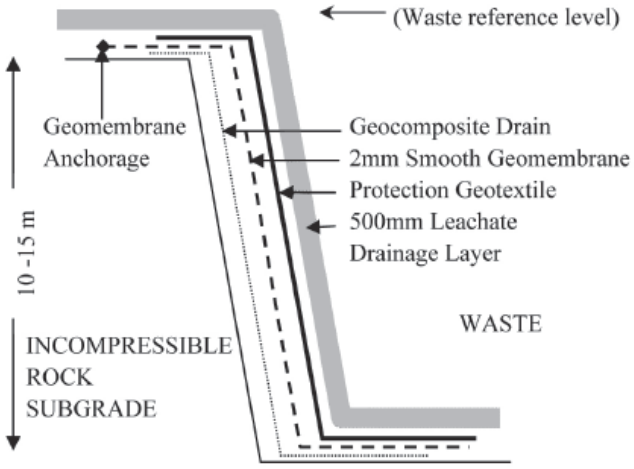

Figure. 2-6 Schematic of lining system used on rock benched subgrade (Fowmes and Dixon, 2005)

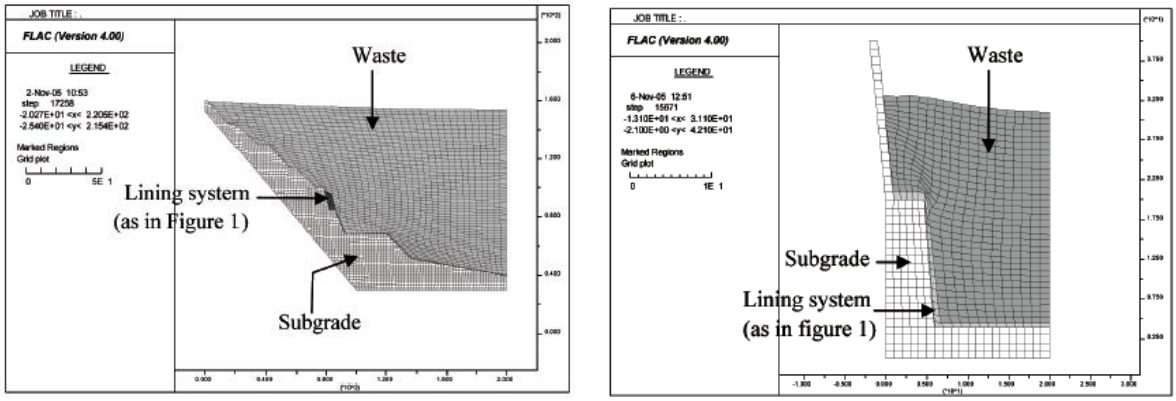

Figure 2-7. Finite difference grid used in the Dixon and Fowmes FLAC landfill models (Fowmes and Dixon, 2005)

Table 2-3. Interface and geosynthetic properties of the Dixon and Fowmes FLAC landfill models (Fowmes and Dixon, 2005)

Interfaces Properties	φ_{peak}	$\varphi_{residual}$
Waste vs. Geotextile	32.0 °	17.0 °
Geotextile vs. Smooth Geomembrane	12.4 °	8.2 °
GCL vs. Smooth/(textured) Geomembrane	13.6 ° (28.7 °)	8.2 ° (14.0 °)
Geosynthetic Properties	Thickness	Young's Modulus
Geotextile	5mm	15MPa
HDPE Geomembrane	2mm	150MPa
GCL	9mm	30MPa

Figure 2-8 illustrates the axial strains and forces developed in geomembrane as predicted in the FLAC analysis. Based on the result of numerical analysis, Fowmes and Dixon (2005) indicated that mobilized forces on the interface above the geomembrane

must not exceed the shear strength mobilized on the interface below the geomembrane in order to prevent development of large tensile force.

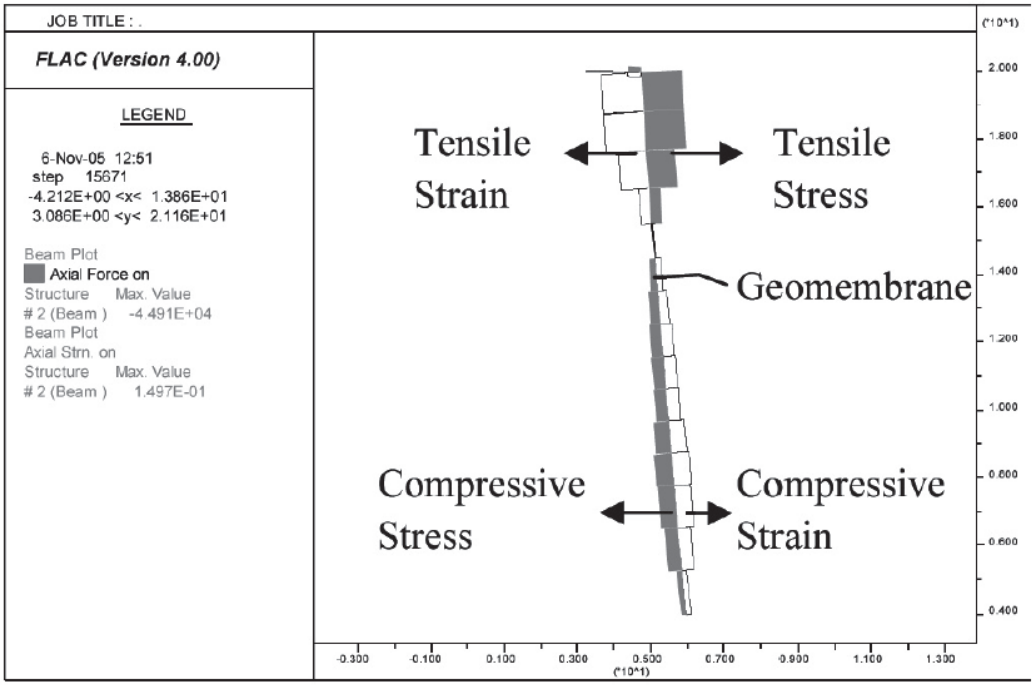

Figure 2-8. The axial strains and forces developed in geomembrane (Fowmes and Dixon, 2005)

2.4 AXIAL STESS-STRAIN BEHAVIOR OF HDPE GEOMEMBRANE

The tensile stress-strain response of HDPE geomembrane was evaluated by Merry and Bray (1996). These investigators performed multiple tests on wide strips of HDPE geomembrane with different aspect (length to height) ratios. Figure 2-9 shows the stress-strain results from tests performed on specimens with aspect ratios from 5.5 (304.8 mm wide × 55.8 mm long) to 0.10 (25.4 mm wide × 254.0 mm long). From their test results, Merry and Bray (1996) found that there was no systematic variation in the stress-strain

response due to changes in the specimen aspect ratio, which indicating that all of the tests yielded the true stress-strain response of the HDPE geomembrane.

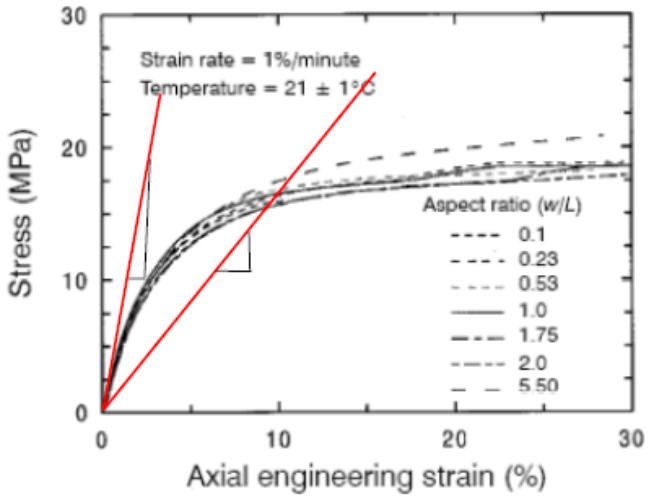

Figure 2-9 Comparison of uniaxial tension test results with different aspect ratios for HDPE geomembrane specimens (Merry and Bray 1996)

Giroud (1993) reported results more than 500 uniaxial tensile tests on HDPE geomembrane specimens from five US manufacturers at temperatures ranging from 20 ℃ to 70 ℃. The data indicated that the stress–strain responses for HDPE geomembrane from different manufacturers are similar. Figure 2-11 (a) shows the average uniaxial stress–strain curves obtained from the HDPE geomembrane test results by Giroud (1993) (only the portion of the curve between the origin and the yield peaks are shown). Giroud (1994) notes that the initial tensile stiffness(modulus) of HDPE geomembrane is three to four times greater the secant modulus at yield of the specimen. Giroud (2005) established the relationships between the geomembrane yield stress (σ_y) and temperature shown in

Figure 2-10 (b) and between the yield strain and the temperature is shown in Figure 2-11 (c).

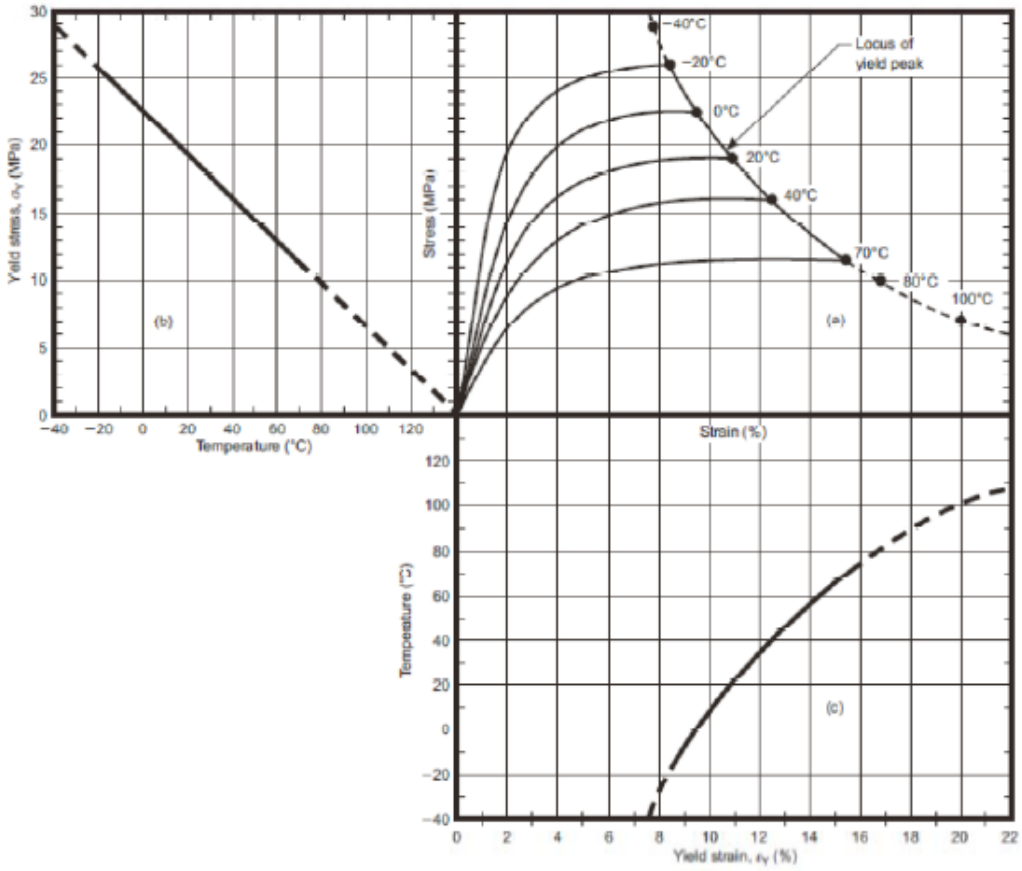

Figure 2-10 Average tensile characteristics of HDPE geomembranes as a function of temperature: (a) uniaxial stress–strain curves from the origin to the yield peak; (b) yield stress as a function of temperature; (c) yield strain as a function of temperature (Giroud 2005)

Giroud (2005) employed an N-order parabola, where N = 4, to develop a normalized stress–strain curve for all of the tested HDPE geomembranes regardless of temperature.

This parabola is shown in Figure 2-11. The equation for the N-order parabola is given by Giroud (2005) as:

$$\frac{\sigma}{\sigma_y} = 1 - \left(1 - \frac{\varepsilon}{\varepsilon_y}\right)^N \tag{2-5}$$

where σ_y is the uniaxial stress at yield, ε_y is the uniaxial strain at yield, and N is 4 for HDPE. In this equation, the dependence of HDPE stress-strain behavior on temperature is captured by the dependence of the normalizing yield stress, σ_y, on temperature. With this equation, the uniaxial stress–strain curve of the geomembrane between the origin and the yield peak can be estimated.

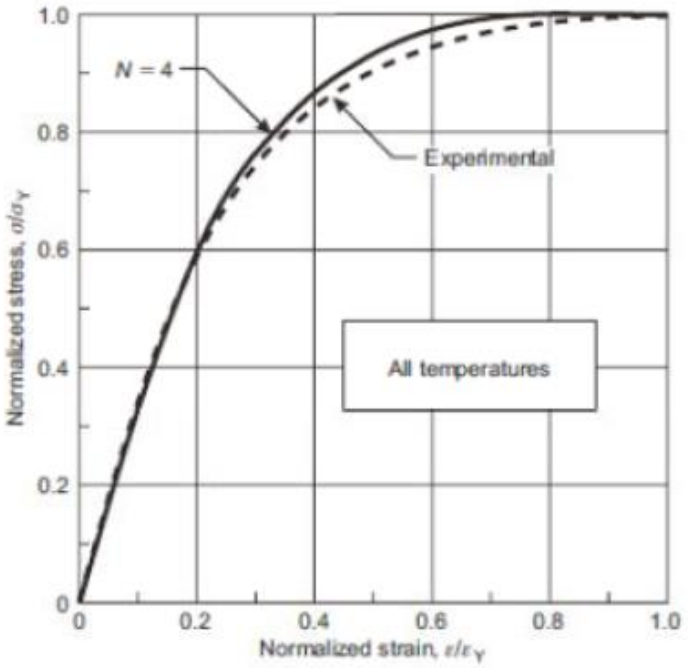

Figure 2-11 HDPE geomembrane normalized uniaxial stress– strain curve, for all temperatures (Giroud 2005)

Using the hyperbolic stress-strain relationship in Eq. 2-5, the relationship between the tangent moduli, E_{tan}, for any strain below the yield strain is given by the following equation developed by Giroud (1994):

$$E_{\tan} = \frac{N\sigma_y}{\varepsilon_y}\left(1-\frac{\varepsilon}{\varepsilon_y}\right)^{n-1} \tag{2-6}$$

The relationship between tangent modulus and axial strain and secant modulus and axial strain for HDPE is given by Eq. 2-6 is shown in Figure 2-12. A significant aspect of the Giroud (1994) N-order parabola is that the initial modulus of an HDPE geomembrane, E_o, is N times the secant modulus at yield, as expressed in the following equation:

$$E_o = N\frac{\sigma_y}{\varepsilon_y} = 4\frac{\sigma_y}{\varepsilon_y} \tag{2-7}$$

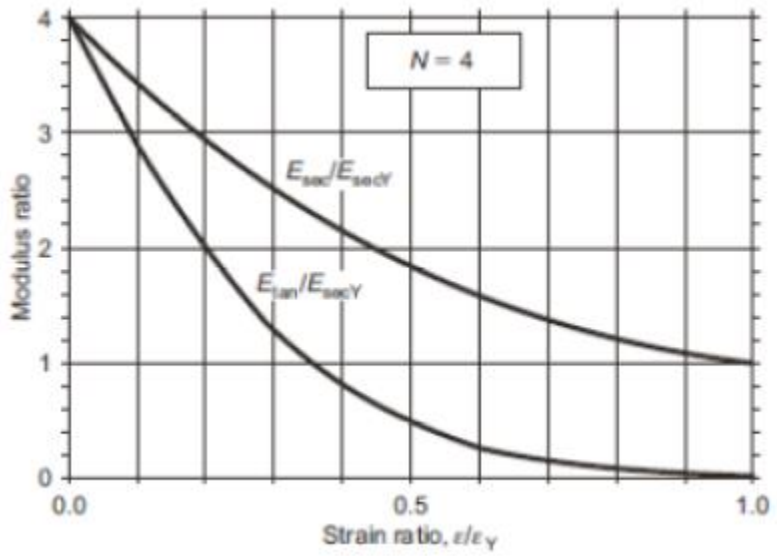

Figure 2-12 Geomembrane uniaxial secant and tangent moduli at any strain below the yield strain (Giroud 2005)

2.5 GEOMEMBRANE STRAIN CONCENTRATIONS

Failure in a geomembrane may occur due to strain (or stress) concentrations even though the average strain (or stress) on the geomembrane is not enough to cause failure. Giroud (2005) classified strain concentrations in geomembranes into two main categories: strain concentration due to scratches in the geomembrane and strain concentration due to bending at the seams. In both cases, the strain concentration is the result of an abrupt change in geometry, i.e. an abrupt change in thickness of the geomembrane due to the seam overlap or due to the penetration of a scratch into the geomembrane. Figure 2-13 and Figure 2-14 illustrate these two types of abrupt geometry change.

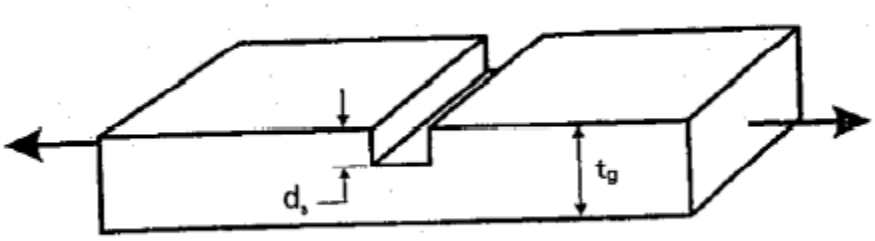

Figure 2-13. Geomembrane with scratch (Giroud 1993)

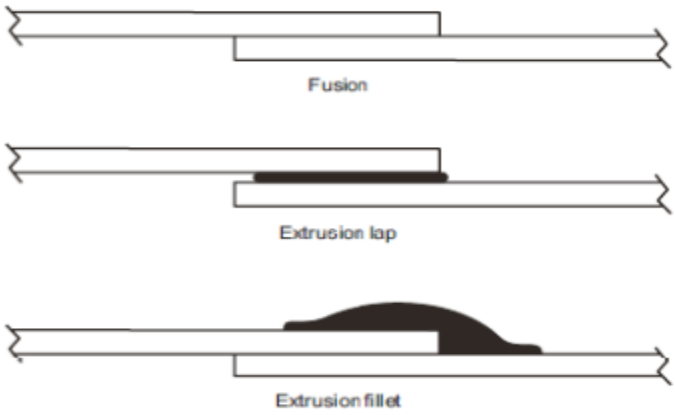

Figure 2-14. Geomembrane seam types, with the extrudate shown in black (Giroud 2005)

2.5.1 Strain concentration due to bending at seams

Giroud (2005) developed strain concetration factors based upon the observation that seams rotate perpendicular to the loading direction when a geomembrane is loaded in tension. The rotation of the seam is due to equilibrium of the tensile forces applied on the geomembrane, which requires a portion of the geomembrane on one side of the seam to be in the same plane with a portion of the geomembrane on the other side. As a result, axial strain is induced in the geomembrane as it bends on each side of the seam, as shown in Figure 2-15.

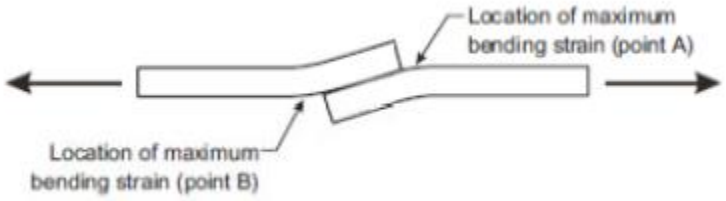

Figure 2-15. Bending strain due to rotation in the seam (Giroud 2005)

Giroud et al. (1995) developed a mathematical relationship for the additional strain that occurs in the geomembrane due to bending of the seam. Figure 2-16, from Giroud (1993) presents the maximum additional strain in the geomembrane due to bending, ε_b, referred to as the 'additional strain due to bending,' as a function of the type of seam, seam thickness, and average strain in the geomembrane. The plots in this figure shows the additional bending strain can range up to 3.5% for typical weld types and thicknesses. These plots suggest that the strain in the geomembrane at the weld will typically be on the order of 2 to 2.25 times the average axial strain developed in the geomembrane.

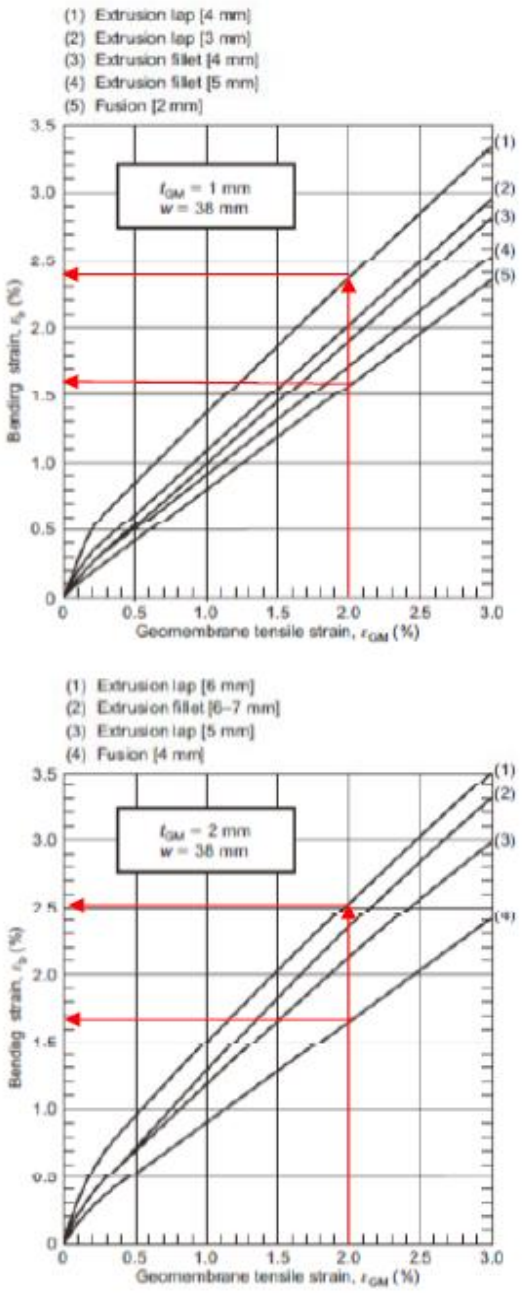

Figure 2-16. Additional strain due to geomembrane bending next to a seam, ε_b, as a function of the tensile strain in the geomembrane away from the seam, GM **(after Giroud 1993)**

2.5.2 Strain concentration due to scratches

Giroud (1993) evaluated that stress concentration around a scratch in a geomembrane. His analysis indicated that the additional strain due to a scratch is proportional to the geomembrane thickness reduction due to the scratch. The ratio between the yield strain of a scratched HDPE geomembrane, ε_{ys}, and the yield strain of an intact HDPE geomembrane, ε_y, is given by the following equation:

$$\varepsilon_{ys} = \varepsilon_y \left(1 - \left(\frac{d_s}{t_{GM}} \right)^{1/N} \right) \tag{2-8}$$

where d_s is the depth of scratch or any other type of thickness reduction, t_{GM} is the geomembrane thickness, and N = 4 for HDPE. This relationship is shown in Figure 2-18. The relationship in Figure 2-18 shows that a scratch as little in depth as 0.1 times the geomembrane thickness can reduce the yield strain in the geomembrane to 45% of the value of a geomembrane without a scratch.

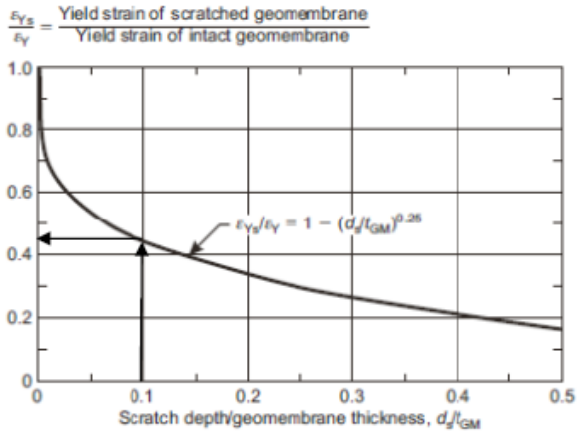

Figure 2-17 Ratio of the yield strains of an HDPE geomembrane with a scratch, or any other type of thickness reduction, and an intact HDPE geomembrane (Giroud 1993)

2.6 ALLOWABLE STRAIN

The allowable strain for an HDPE geomembrane is the function of multiple factors includes the yield strain of material, global strain, strain concentrations, plane strain effects and the factor of safety. Arab (2011) found the allowable strain could be as low as 3-4% if the yield strain for an HDPE is 11-14%.

CHAPTER 3 NUMERICAL MODELING OF MSW BEHAVIOR

3.1 INTRODUCTION

The modeling tool employed in this dissertation is FLAC 7.0, a large strain finite difference computer program for evaluation of stresses and strains in continuous (geologic) media. In order to achieve the goals of this thesis, the mechanical behavior of MSW during and after placement of waste must be modeled in FLAC 7.0. FLAC 7.0 has the following built-in constitutive material models for continuous media: isotropic and transversely isotropic elastic models and nine plasticity models: Drucker-Prager and Mohr- Coulomb elastic-perfectly plastic, Ubiquitous-Joint, Strain-Hardening/Softening, Bilinear Strain Hardening/Softening Ubiquitous-Joint, Double-Yield, Modified Cam-Clay, Hoek-Brown, and Cap-Yield (Cysoil). The constitutive model that was used in this study to describe the behavior of MSW is the Modified Cam-Clay (MCC) model.

3.2 MODIFIED CAM-CLAY MODEL

The Modified Cam-Clay model is an incremental elasto-plastic constitutive model developed to describe the behavior of soft compressible soils. The model's features include a nonlinear hardening behavior governed by volumetric plastic strain.

Three state variables are employed in the Cam-Clay model: the mean effective pressure, p, the deviator stress, q, and the specific volume, v (v =1+e, where e = void ratio). In FLAC 7.0, the principal stresses, σ_1, σ_2 and σ_3 are used to define p and q and, by

convention, tension, traction, and dilation are positive. The state variables p and q are defined in FLAC as:

$$q = -\frac{1}{\sqrt{2}}\sqrt{(\sigma_1 - \sigma_2)^2 + (\sigma_2 - \sigma_3)^2 + (\sigma_1 - \sigma_3)^2} \quad (3\text{-}1)$$

$$p = -\frac{1}{3}(\sigma_1 + \sigma_2 + \sigma_3) \quad (3\text{-}2)$$

3.2.1 Virgin consolidation line and swelling lines

In the Cam-Clay model, the relationship between the normal stress and the specific volume is defined by isotropic or one dimensional compression test results. For example, Figure 3-1 shows the results of an isotropic compression test. The isotropic compression curve in Figure 3-1 is characterized by two lines: the virgin consolidation line (which is parallel to the K_0 compression line in a one-dimensional compression test) and the swelling (or rebound) line.

The virgin consolidation line in Figure 3-1 is defined by the following equation:

$$\upsilon = \upsilon_\lambda - \lambda \ln p \quad (3\text{-}3)$$

where ν_λ is the specific volume on the virgin compression line at p = 1.

The equation for the swelling line is:

$$\upsilon = \upsilon_{\kappa} - \kappa \ln p \qquad (3\text{-}4)$$

where ν_κ is the specific volume on the swelling line at p = 1.

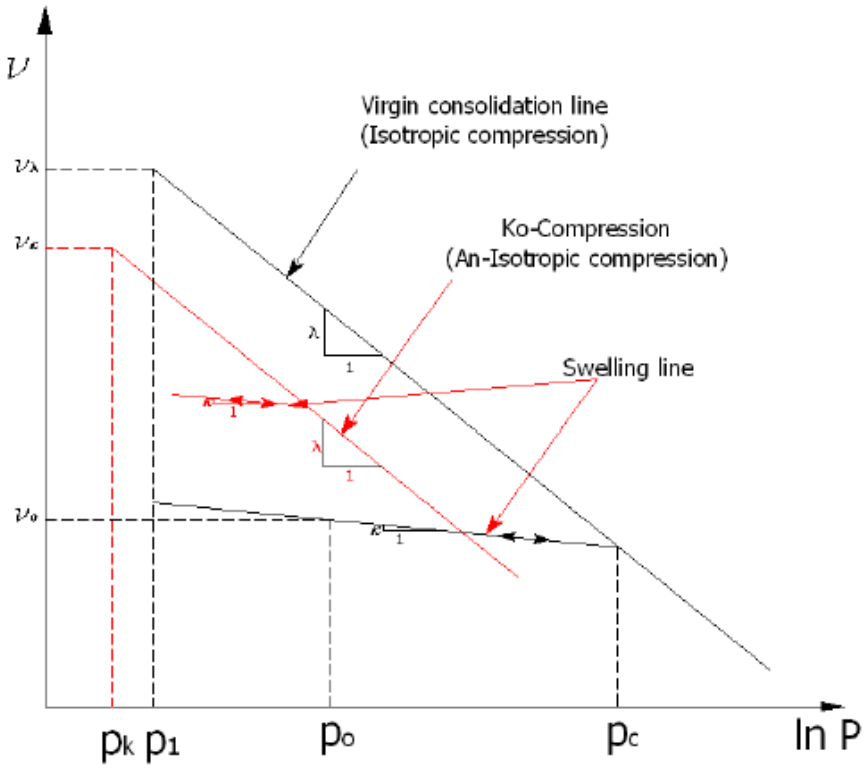

Figure 3-1 Isotropic compression curve used in Cam-Clay and the relationship with the 1-D K_0 compression test constitutive model

The virgin consolidation and swelling lines for one-dimensional compression are assumed to be parallel to the corresponding lines in isotropic compression (i.e. κ and λ in one-dimensional compression are assumed to be the same as in isotropic compression)

3.2.2 Yield Functions

In the Cam-Clay model, the soil behaves elastically until the yield value of q is attained. The yield value of q is determined from the following equation:

$$f = q^2 + M^2 p(p - p_c) \qquad (3\text{-}5)$$

where M is a material constant and p_c is the preconsolidation pressure (sometimes called the maximum past pressure, and illustrated in Figure 3-1). The yield condition f= 0.0 is represented on a p-q plot by an ellipse oriented with one axis along the horizontal (p) axis and with a peak located along a line through the origin with a slope of M, as shown in Figure 3-2.

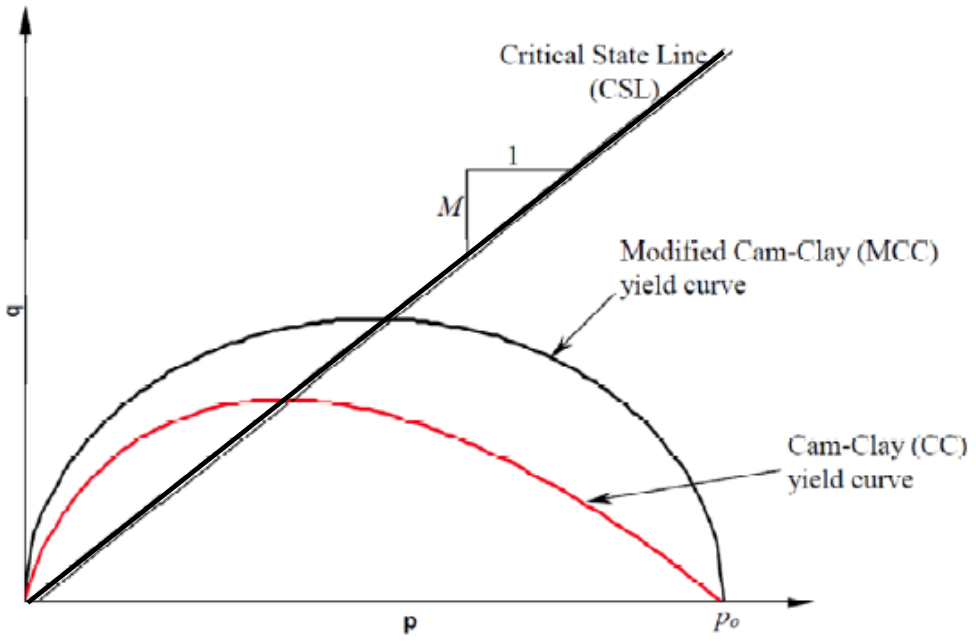

Figure 3-2 Cam-Clay and Modified Cam-Clay yield surfaces (in p-q) space. The parameter M is the slope of the CSL (Rockscience 2005)

3.2.3 Hardening and Softening Behavior

The line through the p-q plot origin with a slope of M (the locus of the peak points of all yield ellipses) is referred to as the critical state line (CSL). If yielding occurs to the right the CSL, hardening behavior is accompanied by volumetric compression. This side of the yield surface is known as the wet, or subcritical, side of the CSL. Figure 3-3 (a) illustrates soil behavior on the wet side of the CSL for the case of direct simple shear loading. When a sample is loaded in shear, it behaves elastically until it hits the initial yield surface. From then on the yield surface begins to isotropically expand and the soil exhibits hardening behavior (yielding and plastic volumetric strain is accompanied by an increase in yield stress). Figure 3-3 (b) shows the hardening deviatoric stress strain behavior that occurs for a sample loaded in simple shear (i.e. is sheared at a constant value of p) on the wet side of the CSL. If yielding occurs to the left of the CSL line, the soil exhibits softening behavior accompanied by dilatancy (volume expansion), as shown in Figure 3-4 (a). When softening, the yield surface contracts after the stress state point touches the initial yield surface. The deviatoric stress-strain curve for softening behavior is shown in Figure 3-4 (b).

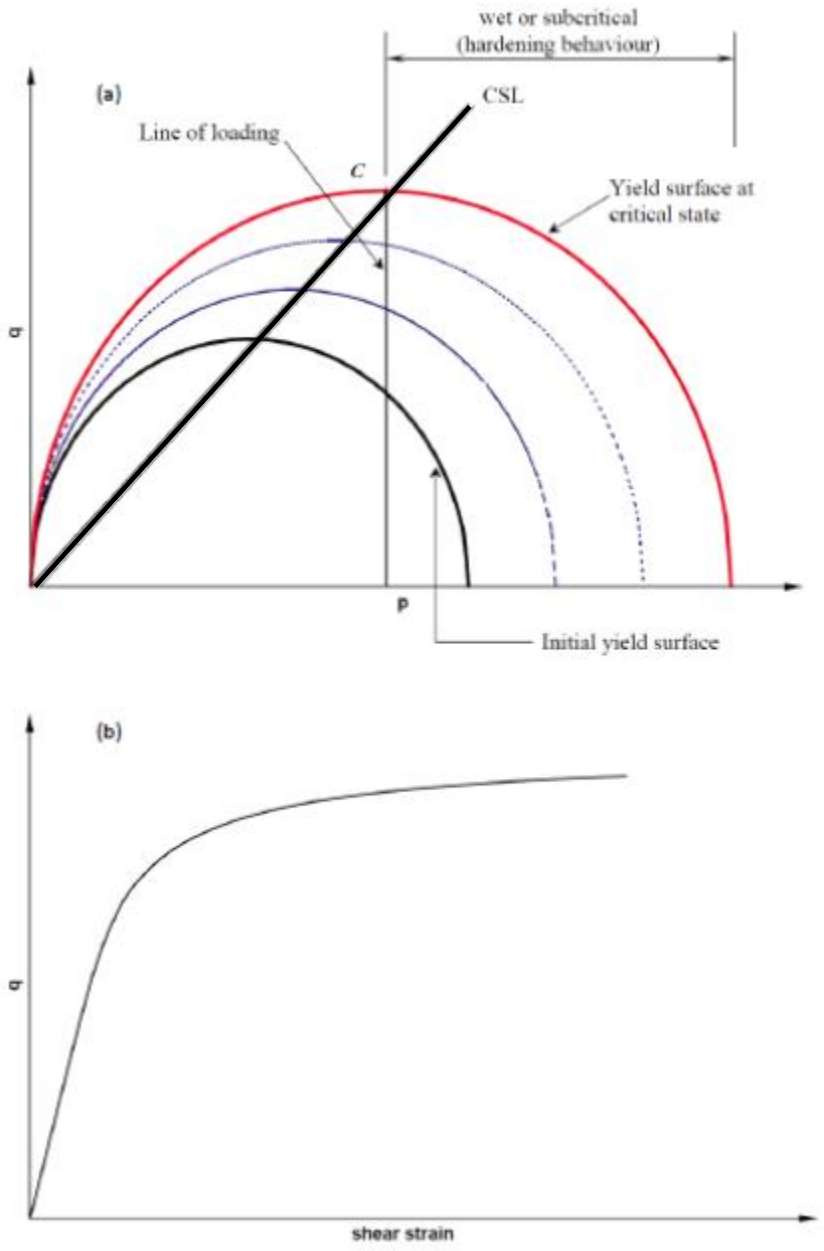

Figure 3-3 Hardening stress behavior, (a) stress path; (b) stress strain behavior (Rockscience 2005)

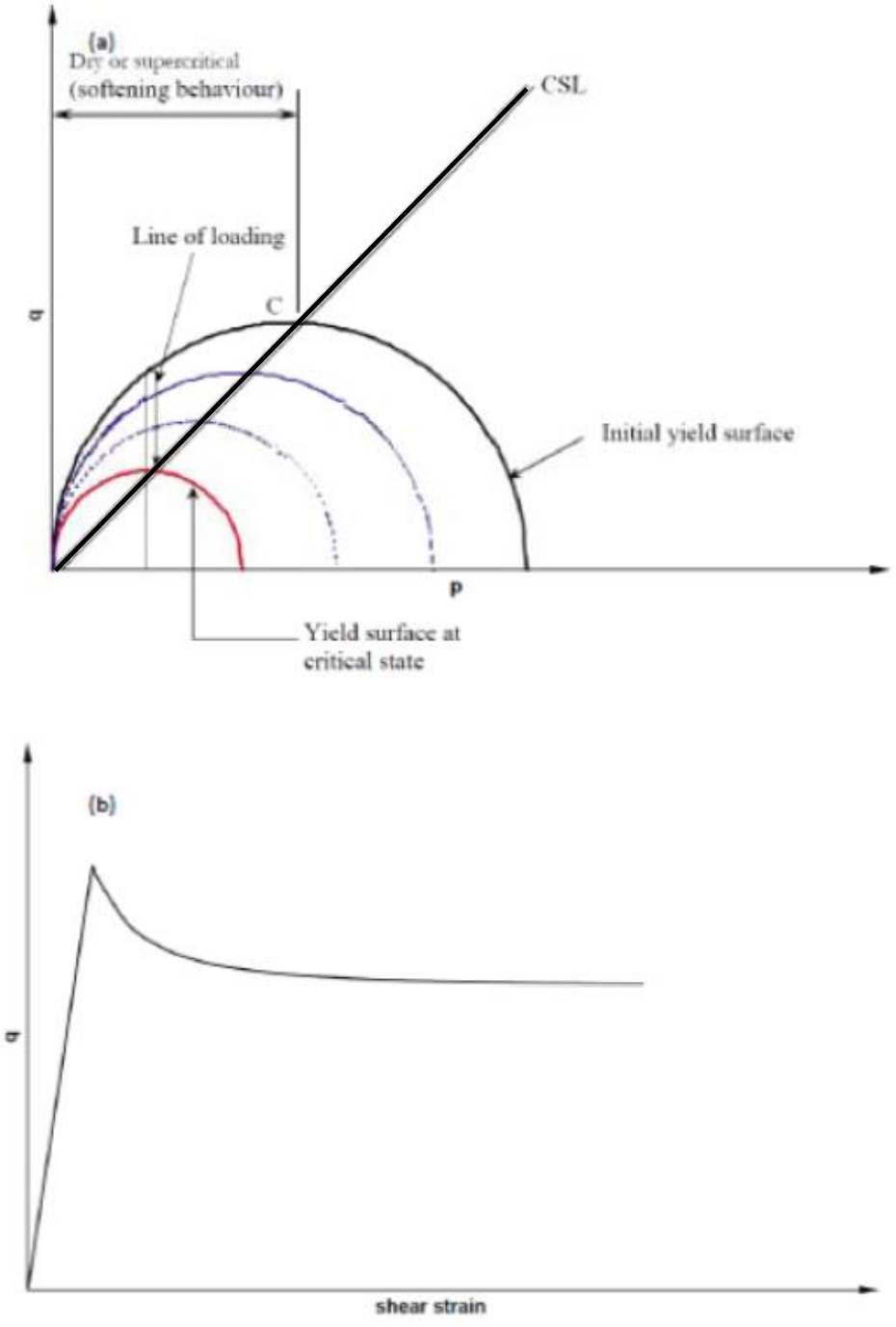

Figure 3-4 Softening Stress behavior, (a) stress path; (b) stress strain behavior (Rockscience 2005)

3.2.4 Elastic material constants for Modified Cam-Clay

For Modified Cam-Clay soils, the bulk modulus, K, is not a constant but instead depends on mean stress, p, the specific volume, v, and the swelling line slope, κ. The bulk modulus is calculated at any point in the soil as:

$$K = \frac{vp}{\kappa} \tag{3-6}$$

Modified Cam-Clay formulations require specification of either the shear modulus *G* or Poisson's ratio υ, but not both. When *G* is supplied, υ is no longer a constant but is calculated from K and G as:

$$\upsilon = \frac{3K - 2G}{2G + 6K} \tag{3-7}$$

3.2.5 Summary of input parameters

The slope of the critical state line, M, can be related to ϕ', the Mohr-Coulomb friction angle of the soil obtained in triaxial compression testing, as:

$$M = \frac{6\sin\phi}{3 - \sin\phi} \tag{3-8}$$

The slope of the virgin consolidation and swelling lines (λ and κ) can be derived from an isotropically consolidated triaxial test or from a one-dimensional compression

test. Note that the slope of the v versus ln p line will be equal to the slope of the e versus ln p line, where e is the void ratio and is related to v as:

$$e = v - 1 \tag{3-9}$$

The slope of the e versus log p virgin compression curve, sometimes called the compression index, C_c, is related to λ and the slope of the e vs. log p swelling curve C_s, sometimes called the recompression or swelling index, related to κ as:

$$\lambda = \frac{C_c}{\ln(10)} \tag{3-10}$$

$$\kappa = \frac{C_s}{\ln(10)} \tag{3-11}$$

3.3 CAM-CLAY PARAMETERS DURING WASTE PLACEMENT

The Modified Cam-Clay (MCC) material properties used to describe MSW during waste placement in FLAC static analyses were derived from a numerical modeling study on the MSW landfill seismic response by Arab (2011). A loading procedure mimicking as closely as practical the assumed waste placement scenario in the field was used to calculate the stresses and deformations in the waste and the forces on and strains of the geomembrane liner. Waste material was placed in horizontal lifts 7 or 8 meters in initial thickness, as shown in Table 3-2, similar to the typical method of landfill operation. Most of the MCC parameters for the waste material used in the research described herein were

the same as in Arab's (2011) research. These parameters were established using the results of odometer tests conducted by GeoSyntec (1995) on OII landfill solid waste material. To model post-closure settlement, the value of λ was changed until the change induced the desired amount of post-closure settlement. The value of κ was also changed to keep the ratio of κ/λ constant. The MCC properties for the waste during construction are summarized in Table 3-1.

Table 3-1 Modified Cam-Clay properties used for waste settlement during construction

MCC Properties of MSW			
Initial Mass Density (kN/m^3)	10.7	Initial Void Ratio, e_0	2.04
Initial Bulk Modulus (MPa)	4000	Slope of Consolidation line, λ	0.086
Initial Shear Modulus (MPa)	30.93	Slope of Swelling Line, κ	0.0086
Friction Angle (°)	33	Preconsolidation Pressure, Pc (kPa)	40
CSL Slope, M	1.4	Poisson Ratio, υ	0.33

The same MCC parameters are applied to each waste layer. The landfill was constructed layer by layer from the bottom to the top. The final waste mass was 80.5 m in height in total (at the middle of the landfill), with 12 layers of waste and a 1 m final cover layer of soil. The total settlement (after placement) of each waste layer is shown in Table 3-2. The total compression of the waste during waste placement was 7.5 meters.

Table 3-2 The total settlement of waste after construction

Waste Layer Number	Original Thickness (m)	Settlement (m)
12	8	0.07
11	8	0.32
10	7	0.46
9	7	0.53
8	7	0.59
7	7	0.67
6	7	0.71
5	7	0.75
4	7	0.78
3	7	0.82
2	8	0.87
1	8	0.93
	Total Settlement = 7.5 m	

3.4 CAM-CLAY INPUT PARAMETERS POST CONSTRUCTION

An important facet of MSW landfill behavior is the large post-closure settlement that occurs after waste placement has ceased. This post-closure settlement is typically on the order of 10 to 20% of the waste thickness and occurs over an extended period time. This additional waste settlement was mimicked by increasing the slopes of consolidation line (λ) in the MCC model for the waste after all of the waste was in place. To achieve a final settlement of 20% of the initial fill height, λ was changed from 0.086 to 0.16. To keep the ratio of λ to κ constant, κ was changed from 0.0086 to 0.016. The additional settlement

due to the alteration of these MCC paramters was 14.0 m in the middle of the waste fill, or approximately 18% of the final waste thickness.

Figure 3-5 shows the specific volume and shear modulus values for the center of the waste fill, calculated using the post-closure parameters in FLAC, as a function of the depth below the surface of the landfill. Specific volume can be converted to unit weight based upon specific gravity (G_s). Reddy et al (2008) measured G_s values of 0.9 to 1.2 for organic-rich MSW. As the waste analyzed by Reddy et al. (2008) had a very high organic content, for this research, a value of 1.5 is assumed for G_s of the waste. Based upon typical values for MSW, a moisture content of around 25% was also assumed to calculate the total unit weight from the specific volume. The total unit weight of the waste, γ_t, was then estimated as $[1/v]\cdot\gamma_w G_S \cdot 1.25$, where v is the specific volume. Figure 3-6 presents the calculated unit weight versus the depth of waste at the end of post-closure settlement plotted versus typical unit weight versus depth curves for MSW from Zekkos et al. (2008). The unit weight profile for the landfill at the end of the post-closure settlement period show reasonable consistency with the recommended unit weight profiles for conventional municipal solid-waste landfills (for low, typical, and high near-surface in-place unit weight) developed by Zekkos et al. (2008).

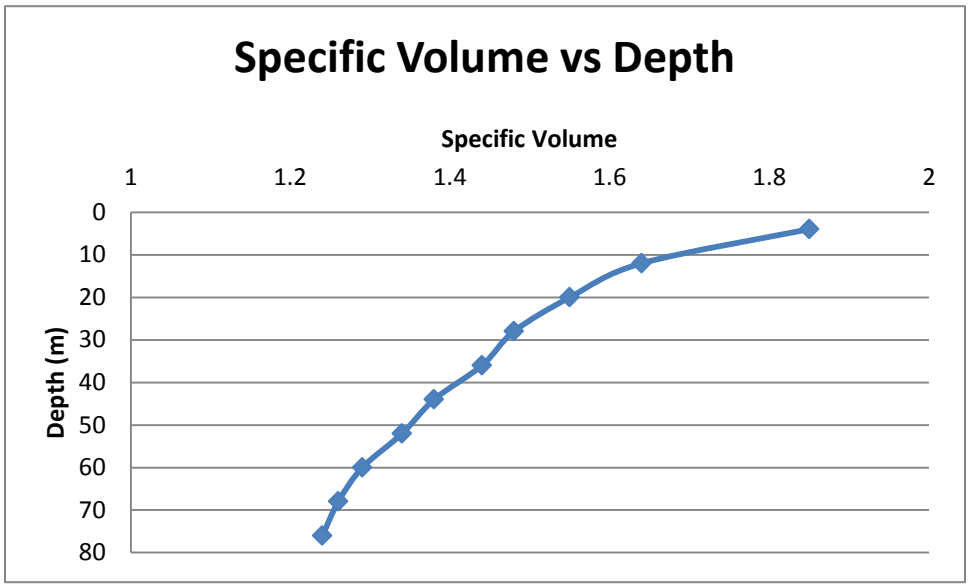

Figure 3-5 The specific volume at the end of post-closure settlement as a function of the depth below the surface of the landfill

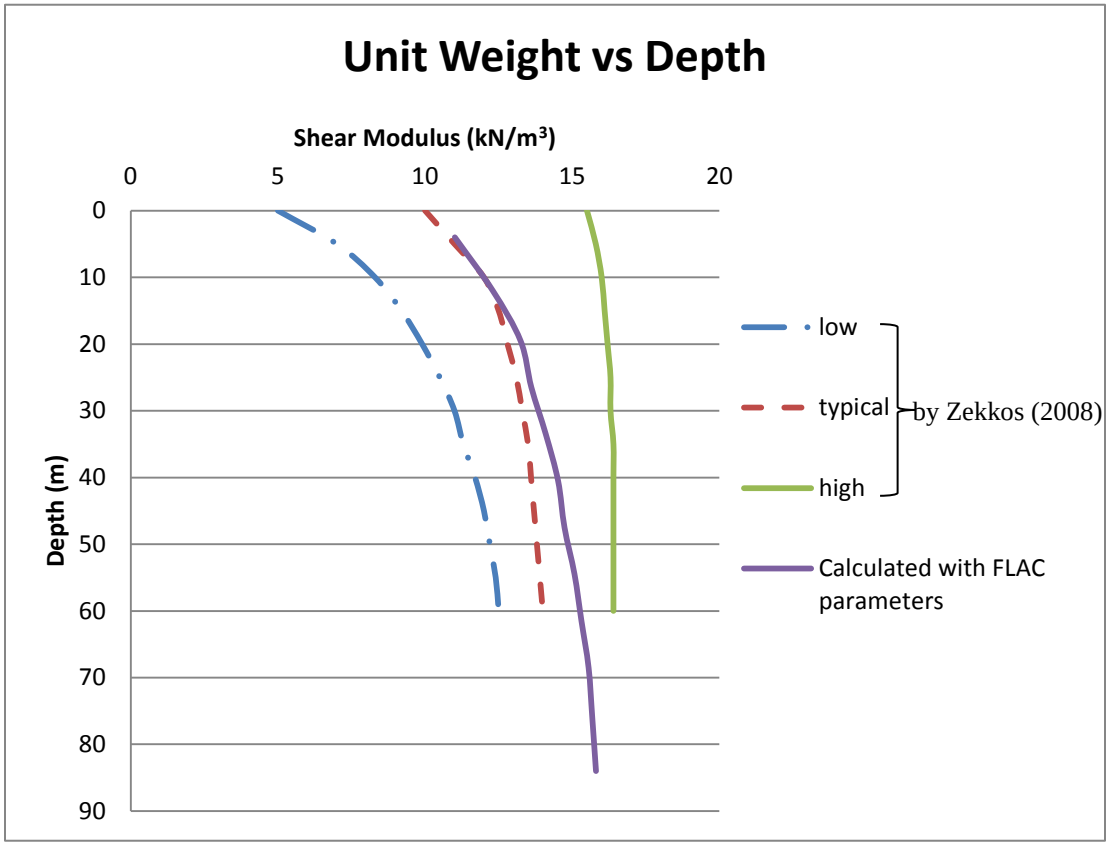

Figure 3-6. The unit weight values assigned to the waste layers as a function of the depth below the surface of the landfill

3.5 MSW PROPERTIES FOR THE DYNAMIC ANALYSIS

For the seismic analysis of the waste fill, the equivalent linear visco-elastic material model was used. This model uses the total unit weight (or specific volume), shear modulus (or Young's modulus) and Poisson's ratio of the soil plus shear strain-dependent modulus reduction and damping curves to describe the behavior of a material subject to seismic loading. Unit weight, shear modulus, and the elastic modulus can be calculated from the MCC input parameters and overburden pressure (or depth within the waste mass). For consistency, these parameters were calculated from the MCC properties

employed in FLAC for the post-closure settlement analysis. Figure 3-7 shows the shear modulus values for the center of the waste fill, calculated using the post-closure parameters in FLAC, as a function of the depth below the surface of the landfill.

Figure 3-8 shows the relationship between the calculated shear wave velocity and depth within the waste fill at the end of the post-closure settlement analysis plotted versus the range of shear wave velocity for southern California solid waste landfills recommended by Kavazanjian et al. (1996). The calculated shear wave velocity values are consistent with, though at the upper end of, the recommended range from Kavazanjian et al., as shown in Figure 3-8.

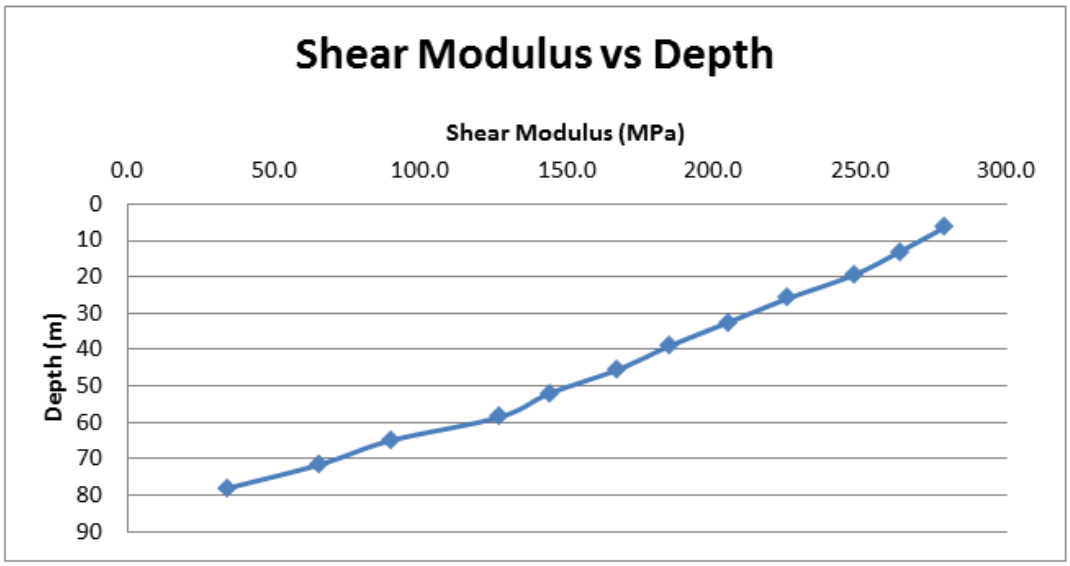

Figure 3-7 The shear modulus assigned to the waste layers as a function of the depth below the surface of the landfill

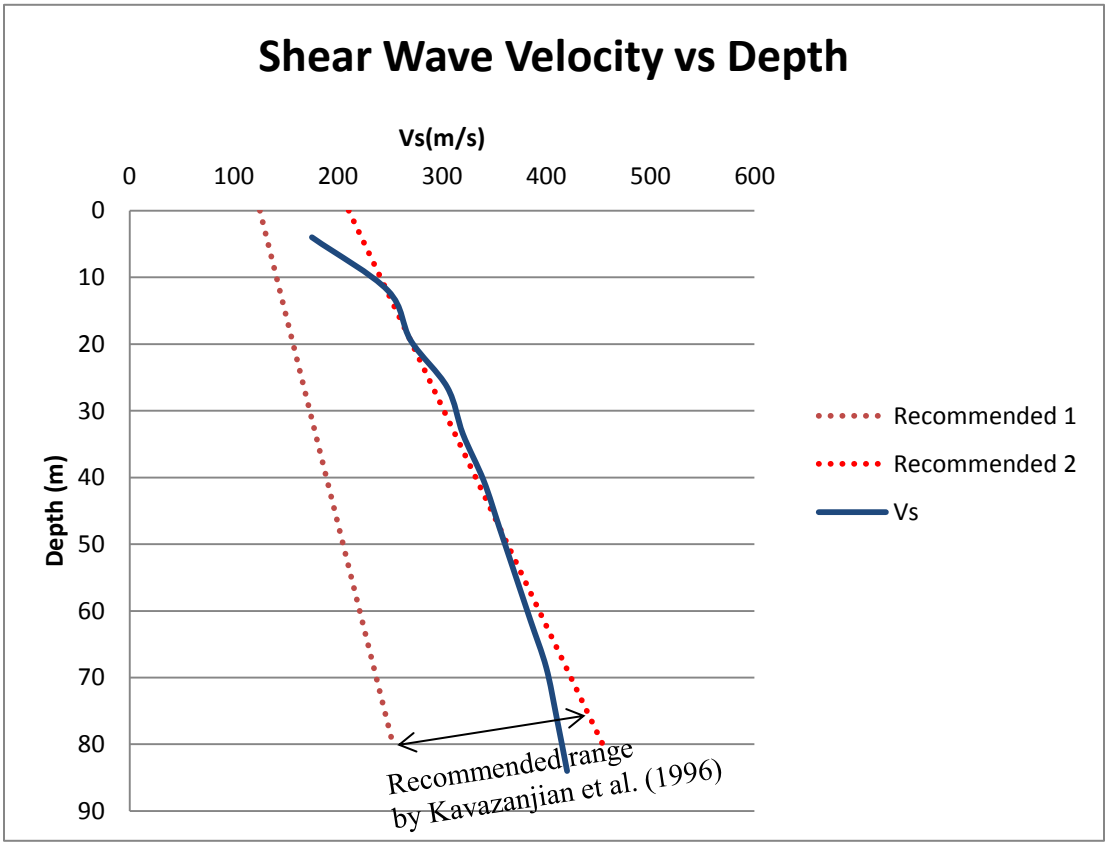

Figure 3-8 The comparison between the calculated shear wave velocity and recommended range of values for southern California solid waste landfills

3.6 CONCLUSION

Cam-Clay material properties for MSW were established based upon oedometer tests by Geosyntec on OII waste and previous values used by Arab. Properties were then adjusted to account for a post-closure settlement of approximately 20% of the waste fill. The resulting unit weight of the waste mass (based upon assumed Gs and w% values) and shear wave velocity agree well with typical values. These properties will be used in the

analysis of geomembrane performance subject to landfill settlement and seismic loading presented in next chapters.

CHAPTER 4 STATIC SETTLEMENT ANALYSIS

4.1 INTRODUCTION

A numerical model was developed in FLAC 7.0 to evaluate the impact of waste settlement on the forces and strains in the geosynthetic elements of Subtitle D – compliant liner and cover systems. The geometry used in the numerical model employed in this research was based upon typical side slope liner geometries for steep-sided canyon landfills in California, e.g. Disposal Area C of the City of Los Angeles Lopez Canyon landfill (Arab 2011). Arab developed a FLAC model to predict the stress-strain behavior of the geosynthetic elements of the Disposal Area C side slope liner system subject to seismic loading from the 1994 Northridge earthquake. In this research, the combined effect of settlement and seismic loading on side slope liner systems of various inclinations as well as on the base liner and cover systems of "typical" southern California canyon landfills was evaluated.

4.2 MODEL GEOMETRY

The finite difference mesh developed to model the side slope liner systems employed in typical canyon landfills is illustrated in Figure 4-1. The mesh has more than 9,000 zones in the foundation, waste mass, and liner and cover systems. In the finite difference model the geomembrane was modeled as a beam element with interface elements on the both sides. For simplicity, only the geomembrane element of the geosynthetic liner and

cover systems were evaluated, e.g. cushion geotextiles, geosynthetic clay liners, and geosynthetic drainage layers were not included in the model. In the analyses reported in this chapter the beam elements were pinned at the top of the slope in the x and y direction to simulate the anchor trench. Four meter-wide benches with a vertical spacing of 13.3 m were employed along the side slope of the model. The slope inclination between benches was 1H:1V (horizontal: vertical) on one side of the model and 2H:1V on the other side of the model so that the influence of slope inclination on liner systems forces and strains could be evaluated. Similarly, the final cover system was modeled using a 3H:1V inclination on one side of the model and a 4H:1V inclination of the other side of the model, with 4 meter-wide benches every 13.3 m, vertically.

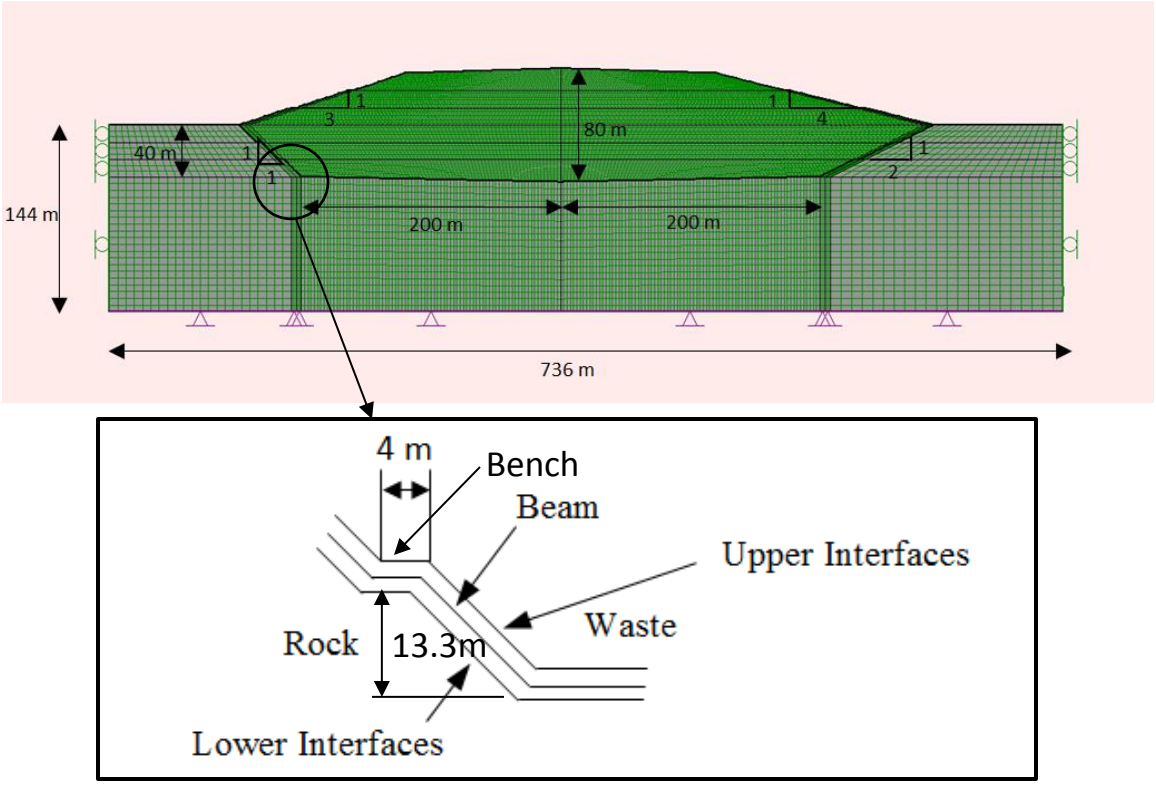

Figure 4-1 Finite difference model employed in the analysis

4.3 WASTE PROFILE AND GEOMEMBRANE PROPERTIES

The impact of static settlement on liner and cover system forces and strains was investigated using the MSW model presented in Chapter 3. Waste was placed in twelve 7 or 8 m lifts up to the final height of the landfill and then the compressibility of the waste was changed to induced post-placement settlement. Figure 4-2 shows the stratigraphy of the finite difference model with 12 layers of waste.

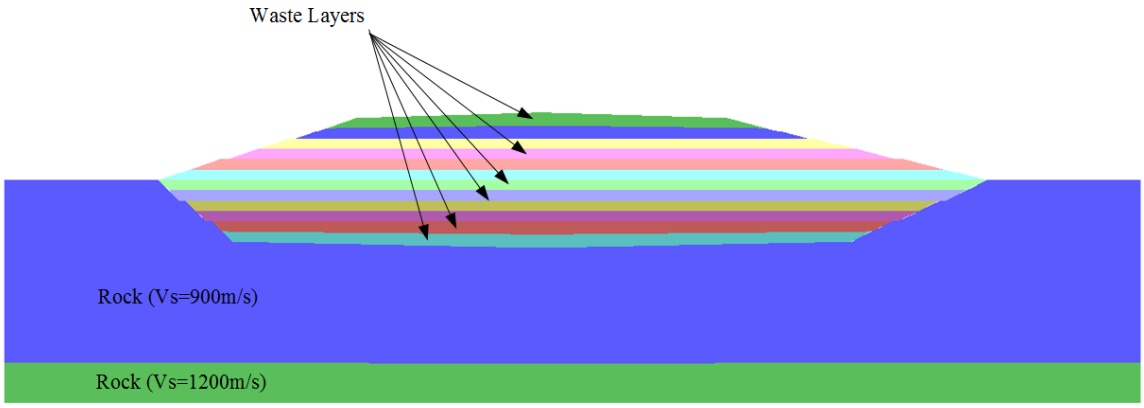

Figure 4-2 Finite difference stratigraphy for static analysis

As illustrated in Figure 4-1, the geomembrane was modeled as a beam element with interface elements on both sides. The lower interface element is rigidly attached to the foundation soil and the upper interface element is rigidly attached to the waste in the geomembrane beam model. For the cover system, the top of the geomembrane was rigidly connected to the overlying soil and only the interface between the bottom of the geomembrane and the underlying waste was considered to evaluate strains in the geomembrane. The in-plane stress-strain behavior of the interface elements was modeled

in FLAC 7.0 as a linear elastic-perfectly plastic Mohr-Coulomb material. Interface behavior is therefore defined using three parameters: the initial stiffness, E_i, and the Mohr-Coulomb shear failure parameters (adhesion, a, and interface friction angel δ). However, for the analyses reported herein the value of a was assumed to be zero. The stiffness assigned to the interface elements in the numerical analysis was 1×10^9 Pa/m based upon the numerical analysis for Chiquita Canyon landfill by Arab (2011). The elastic modulus of the geomembrane was assumed to be 4.84×10^8 Pa/m, representative of a 1.5 mm-thick HDPE geomembrane (Arab 2011). Three different sets of upper and lower interface shear strengths were employed in the numerical analysis to evaluate the inpact of these parameters on geomembrane forces and strains. Table 4-1 presents these three sets of parameters.

Table 4-1 Interface properties used in the analysis

Test Number	Liner		Cover
	Lower Interface Friction Angle	Upper Interface Friction Angle	Interface Friction Angle
1	10 °	20 °	15 °
2	16 °	20 °	
3	25 °	15.5 °	

4.4 STRAINS IN LINER AND COVER SYSTEM ELEMENTS

The axial strains and forces in the geosynthetic liner system elements due to waste settlement were monitored twice: once right after the final waste layer was placed and

again after the post-placement waste settlement had occurred. The cover system is not placed until the end of waste placement, so only the strains induced by post-closure settlement were evaluated in the analysis. The geomembrane liner are constructed by three steps, it was anchored (pinned to the grid element) by the end of the first bench before the first two waste layers placed, and after the next waste layer placed the pinned connections were freed. Then the second and third section of geomembrane was respectively anchored to the end of second and third bench, in the similar manipulation for the first one.

4.4.1 Axial tensile strains & forces in liner

Figure 4-3 shows the axial strains in the liner after the end of waste placement. Three different runs for upper and lower interface shear strengths were employed in the numerical analysis and the results are illustrated in (a), (b) and (c). Figure 4-4 illustrates the axial strains in the liner after the post-closure settlement has occurred. Table 4-2 summarizes the maximum tensile strains in the liner for side slope inclinations of 1H:1V and 2H:1V. As illustrated in Figures 4-3 and 4-4 and by the data in Table 4-2, the greater the value of $\Delta\tan\phi$ (i.e. the greater the difference between the tangent of the upper interface friction angle, $\tan\phi_U$, and lower interface friction angle, $\tan\phi_L$), the greater the strains and forces in the liner system elements.

Table 4-2 Tensile strains in the geomembrane of liner system

Run Number	Lower Interface Friction Angle ϕ_L	Upper Interface Friction Angle ϕ_U	$\Delta\tan\phi = \tan\phi_U - \tan\phi_L$	Maximum Tensile Strain (End of Placement) (%)		Maximum Tensile Strain (Post Placement Settlement) (%)	
				1H:1V	2H:1V	1H:1V	2H:1V
1	10 °	20 °	0.188	8.3	1.9	19.3	3.9
2	16 °	20 °	0.077	3.5	1.0	9.7	1.8
3	25 °	15.5 °	-0.188	1.1	0.3	2.2	0.8

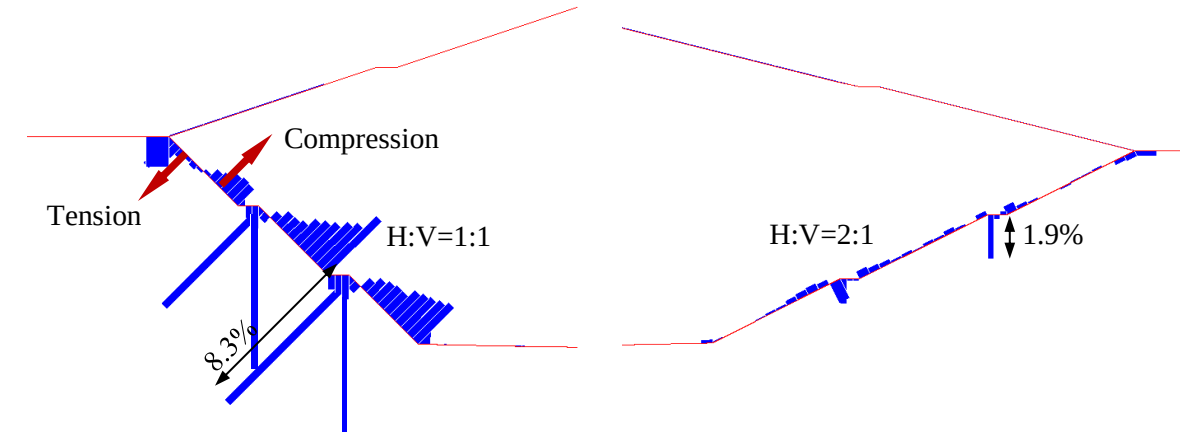

(a) Run No. 1

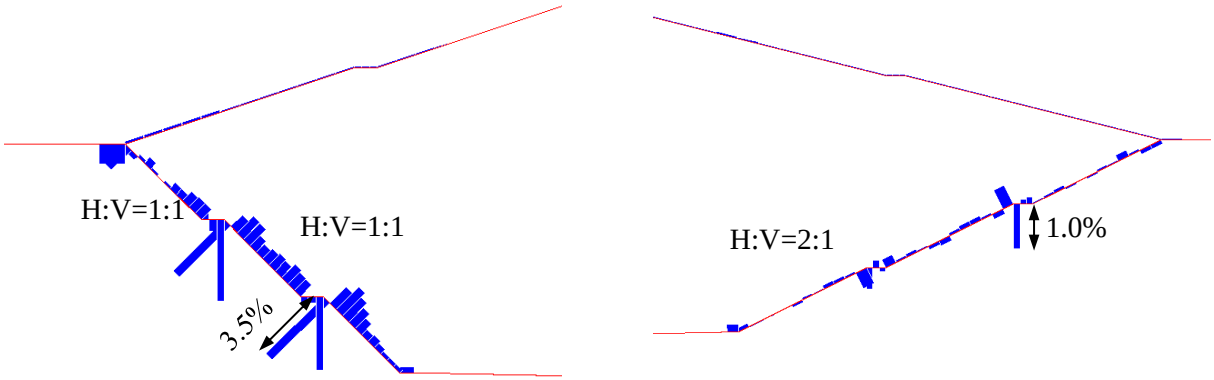

(b) Run No. 2

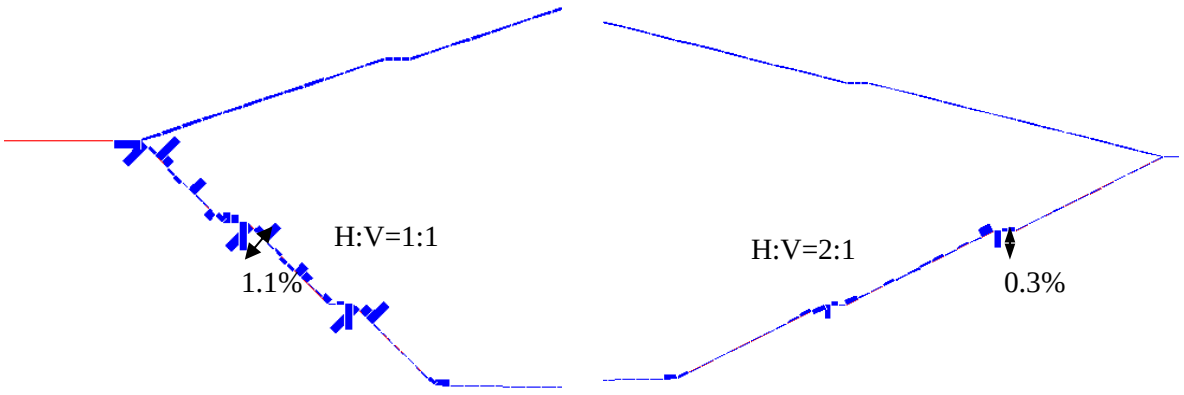

(c) Test No. 3

Figure 4-3 Axial strains in the liner after all the waste layers constructed: a) ϕ_L = 10 °, ϕ_{II} = 20 °; b) ϕ_I = 16 °, ϕ_{II} = 20 °; c) ϕ_I = 25 °, ϕ_{II} = 15.5 °

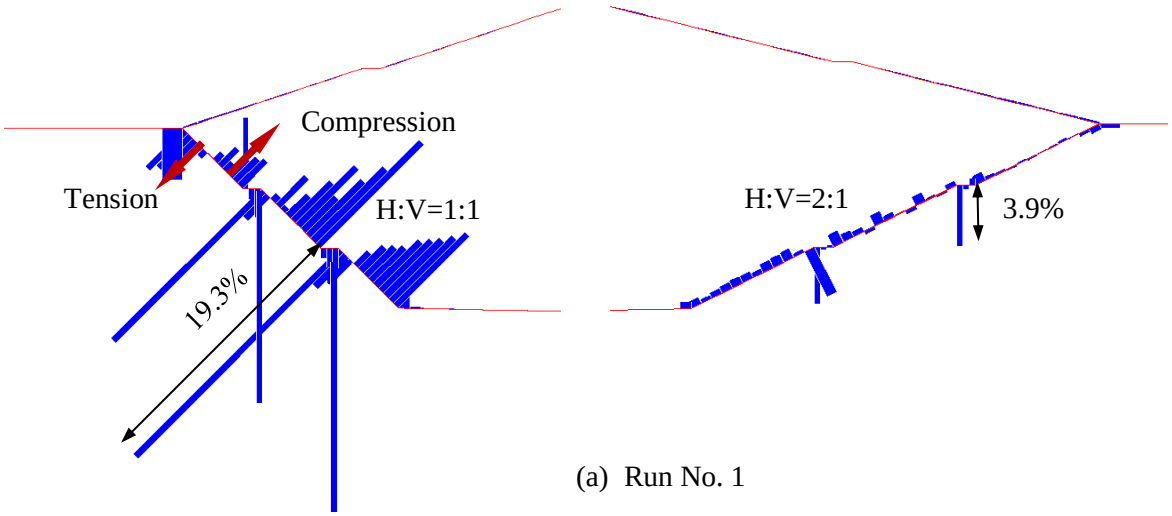

(a) Run No. 1

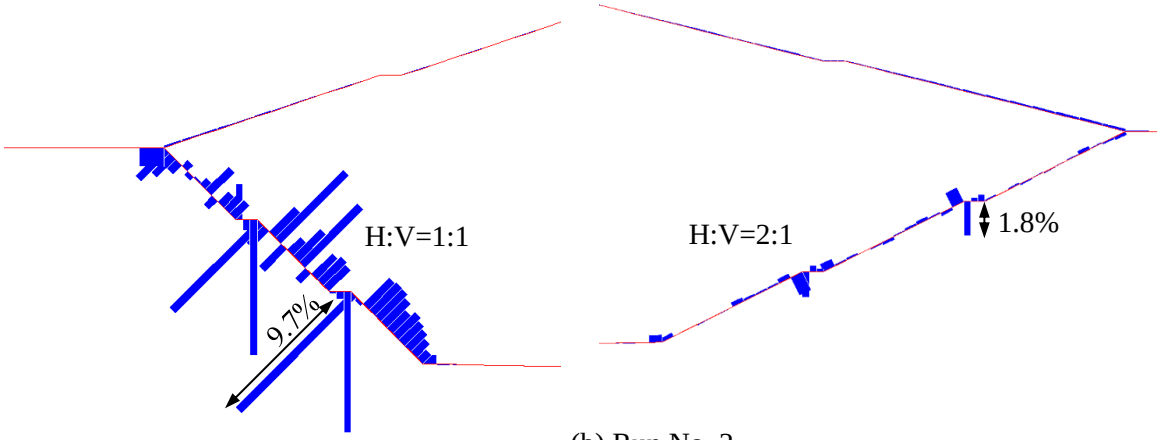

(b) Run No. 2

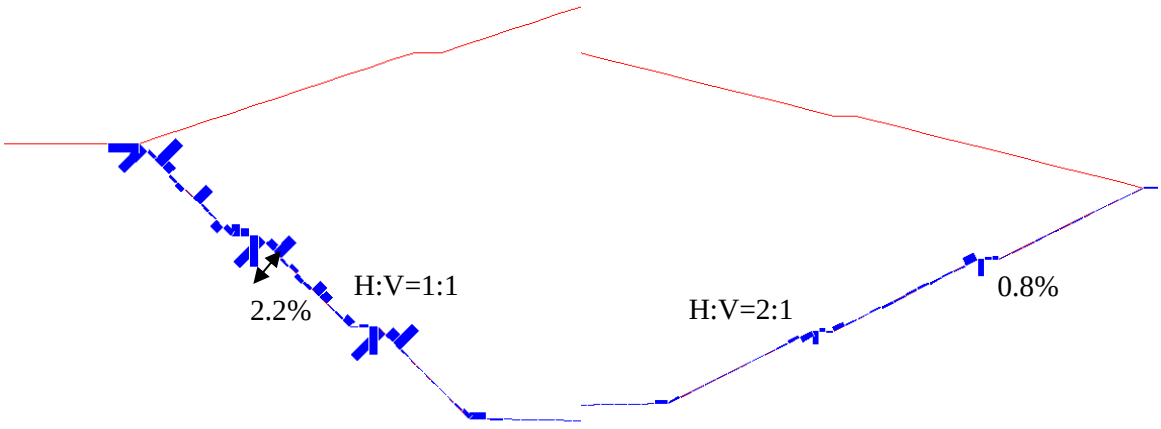

(c) Run No. 3

Figure 4-4 Axial strains in the liner after post-placement settlement: a) ϕ_L = 10 °, ϕ_U = 20 °; b) ϕ_L = 16 °, ϕ_U = 20 °; c) ϕ_L = 25 °, ϕ_U = 15.5 °

4.4.2 Axial tensile strains in cover

To maintain the integrity of geosynthetic barrier on top of waste, the forces and strains in the geosynthetic cover system induced by the waste post placement settlement need to be considered. As opposed to modeling of the side slope liner behavior, only one interface was modeled for the cover system, the interface between the geosynthetic beam and the underlying waste, (typically, either a foundation or low permeability soil layer), as illustrated in Figure 4-5. In other words, the deformation of the geomembrane was assumed to conform to the settlement profile of the waste mass. This is considered a worst-case scenario, as any relative displacement is likely to reduce the strain and force in the geomembrane. Also, as the cover is not placed until waste placement was complete, only the impact of the post-placement settlement was considered.

The final strains induced in the cover system by post-placement waste settlement for the cases considered herein are shown graphically in Figure 4-6. The maximum tensile strains are summarized in Table 4-3 for the three interface strengths considered in the analysis.

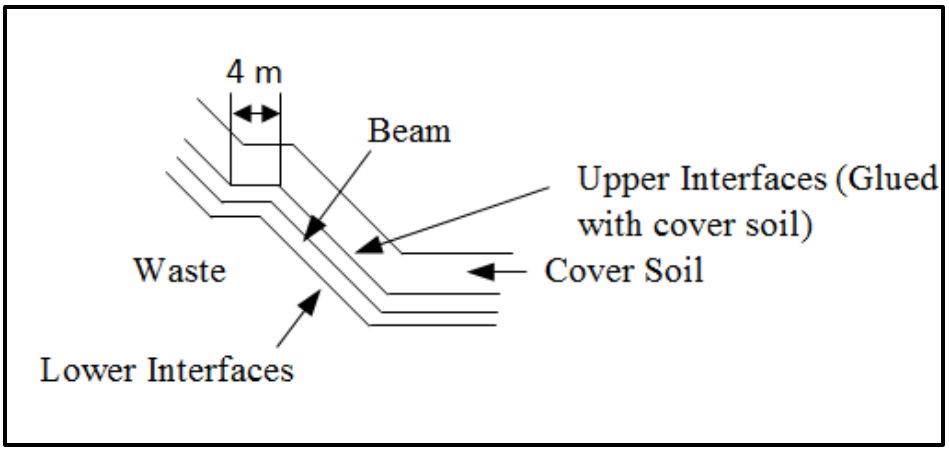

Figure 4-5 Interfaces of cover beam elements

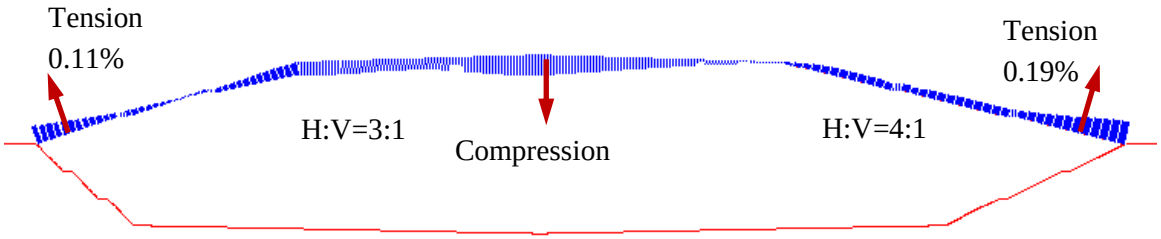

Figure 4-6 Axial strains in the cover due to post placement settlement

Table 4-3 Tensile strains in the geomembrane of cover system

Test Number	Lower Interface Friction Angle ϕ (Upper Glued)	Tensile Strains (Post Settlement) (%)	
		3H:1V	4H:1V
1	15 °	0.11	0.19

4.5 SUMMARY OF THE STATIC SETTLEMENT ANALYSES

A numerical model of a typical southern California canyon landfill, with different side-slope angles on either side of the model, was developed in FLAC 7.0 to evaluate the impact of waste settlement on the forces and strains in geomembrane liner and cover systems. Side-slope angles of 1H:1V and 2H:1V (in between the benches) were investigated. The cover system was evaluated for slope angles of 3H:1V and 4H:1V (between benches). The geomembranes were modeled as beam elements with zero moment of inertia and three different cases of lower and upper interface friction angle were employed for the liner system in the model.

Results of the FLAC 7.0 analyses show that the tension in the liner system was always focused on benches and top of slope. The bottom of each section (between benhes) of side slope slope liner was always in compression. The results also indicate that the axial strains and forces in the systems are sensitive to the slope inclination and the upper and lower interface shear strength (friction angle). The tension in the liner system geomembrane was least when the upper interface friction angel was lower than the lower interface friction angel. However, there was still significant tension in the side slope liner, even when the upper interface shear strength was less than the lower interface shears strength, following post-closure settlement. For the case of $\phi_U < \phi_L$ (i.e. for $\phi_U = 15.5^o$ and $\phi_L = 25.5^o$), the maximum tension after post-closure settlement was 2.2% for the 1H:1V slope, but only 0.8% for 2H:1V slope. Tension for the case of $\phi_U > \phi_L$ depended on

$\Delta\tan\phi$ and the absolute values of ϕ. However, for the 1H:1V slope, tension was very large (e.g. 10-20%) for both cases investigated, which was clearly unacceptable. For the 2H:1V slope, the maximum tensile strain of 1.8% for $\phi_U = 20^o$ and $\phi_L = 16^o$ (the lower $\Delta\tan\phi$ value) would be acceptable (assuming no incremental strain from seismc loading) while the maximum strain of 3.9% for for $\phi_U = 20^o$ and $\phi_L = 16^o$ (the higher $\Delta\tan\phi$ value) is a marginal value for landfill design.

For the cover system, the strains induced by waste settlements were much lower than in liner. The maximum tensile strain in the cover geomembrane on the 4H:1V slope was 0.19%, while the maximum tensile strain on the 3H:1V slope was 0.11%. Both values are clearly acceptable values for landfill design.

CHAPTER 5 SEISMIC ANALYSIS

5.1 INTRODUCTION

In this chapter, the combined impact of settlement and seismic loading on the strains and forces in the geomembrane elements of the representative steep side slope landfill cross section analyzed in Chapter 4 is investigated. The seismic loading is applied at the end of the post-closure settlement period, i.e. the seismic strains are induced on top of the strains induced in the side slope geomembrane liner due to settlement during waste placement and post-closure settlement and on top of the strains induced in the cover system geomembrane due to post-closure settlement.

This chapter first provides a description of the analytical techniques employed in the seismic analysis along with a summary of the dynamic properties of the soil and waste fill materials employed in the analysis. Then, the analyses of the strains and forces in the geomembrane elements of the landfill barrier systems subject to a strong motion record from the Northridge event at the end of the post-closure settlement period using the finite difference computer program FLAC 7.0 is presented.

5.2 INPUT MOTION

Arab (2011) used FLAC 6.0 to evaluate case histories of the performance of the Lopez Canyon and Chiquita Canton landfills in the Northridge earthquake. The Lopez Canyon landfill was subjected to the strongest shaking of the two case histories. The

Lopez Canyon landfill is located fairly close to the Pacioma Dam Downstream strong motion recording station, so the recorded Pacioma Dam Downstream motions from the 1994 Northridge earthquake were used for the Lopez Canyon case history analysis. Due to the proximity of the recording station to the landfill, the strong motion records from Pacoima Dam Downstream station were assumed to represent rock outcrop motions at the Lopez Canyon landfill site. However, the accelerograms were rotated to obtain the motion corresponding to azimuths of 60 degrees and 290 degrees to coincide with the directions of the two cross sections of the landfill analyzed by Arab (2011).

Figure 5-1 shows the response spectra for the motion at the Pacioma Dam Downstream strong motion station rotated to azimuths of 60 degrees and 290 degrees. Due to the proximity of the landfill site to the Pacoima Dam Downstream station, the ground motions at the landfill site were assumed to have the same PGA as recorded at the Pacoima Dam Downstream station. These values were 0.49 g and 0.33 g for the 60 degree and 290 degree azimuth records, respectively. The stronger motion, the record for the 60 degree azimuth with a 0.49 g PGA, was employed in the analysis reported herein. To transform this bedrock outcrop strong motion record into a subsurface ground motion that can be applied at the base of the two-dimensional (2-D) FLAC 7.0 model used in this analysis a deconvolution procedure was employed. The deconvolution procedure used SHAKE2000 to calculate the upward propagating motion at the base of the 2-D FLAC

7.0 model according to the procedure described by Mejia and Dawson (2006). This deconvolution procedure is illustrated in Figure 5-2.

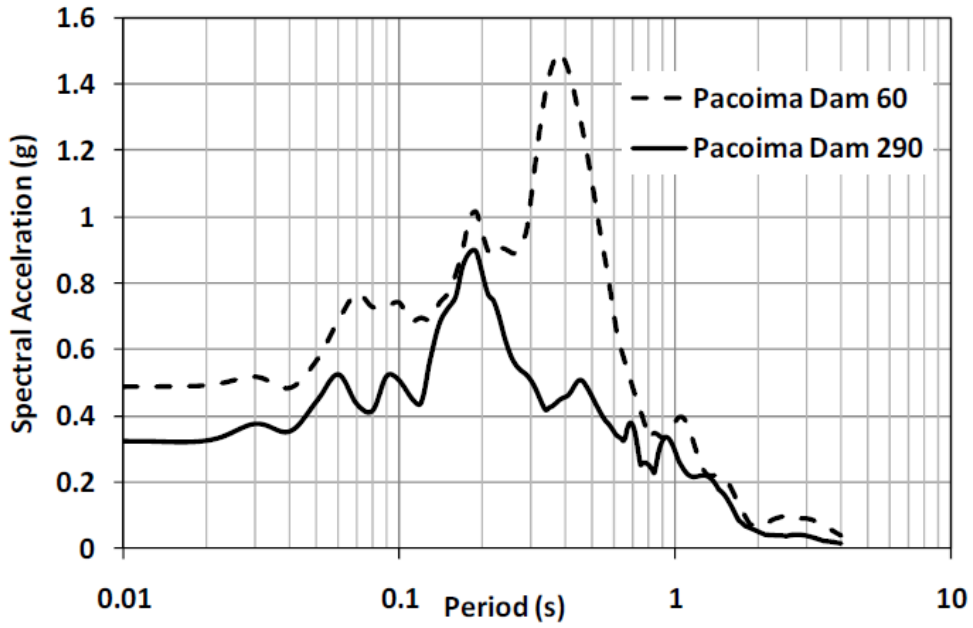

Figure 5-1 Response spectra of motions records at Pacioma Dam Downstream station from 1994 Northridge earthquake rotated to azimuths of 60 degrees and 290 degrees (Arab 2011)

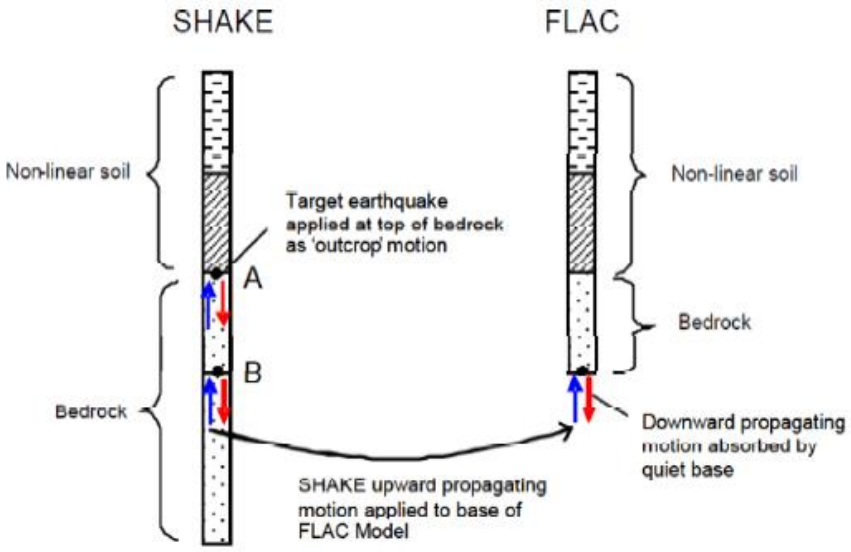

Figure 5-2 The deconvolution procedure for FLAC 7.0 (Mejia and Dawson 2006)

5.3 WASTE PROPERTIES

The unit weight and shear wave velocity of waste for the dynamic analysis were the values at the end of the post-closure settlement period calculated based on the MCC parameters discussed in Chapter 3. These values are presented in Figures 3-6 (for total unit weight) and 3-7 (for shear wave velocity). A value of 0.33 was used for the Poisson's ratio of the waste based upon field measurements at the Operating Industries, Inc. landfill (Matasovic and Kavazanjian 1998). Table 5-1 summarizes the values of total unit weight, shear wave velocity, and Poisson's ratio employed for the waste and foundation rock in the seismic analyses. The waste in the FLAC 7.0 seismic analyses was treated as a nonlinear hysteretic material using back bone curves fitted as discussed subsequently.

Table 5-1 Waste and foundation material properties

	Layer	Unit Weight (kN/m^3)	Shear Wave velocity (m/s)	Poison's Ratio
MSW	1	11.0	175	0.33
	2	12.3	248	0.33
	3	13.2	270	0.33
	4	13.6	305	0.33
	5	14.1	320	0.33
	6	14.5	340	0.33
	7	14.7	355	0.33
	8	15.1	370	0.33
	9	15.3	385	0.33
	10	15.6	400	0.33
	11	15.7	410	0.33
	12	15.8	420	0.33
Rock	1	16.5	900	0.25
	2	18.8	1200	0.25

Shear modulus reduction and damping curves for the waste in the FLAC analysis were derived from the backbone curve. A functional form was assumed for the waste backbone curve based upon the FLAC subroutine called "Hardin/Drnevich model." The resulting shear modulus reduction and damping curves were compared to the corresponding curves for MSW recommended by Matasovic and Kavazanjian (1998) based upon back analysis of the seismic response of the Operating Industries, Inc. landfill in southern California. The parameters describing the backbone curve were adjusted until relatively good agreement was achieved for both the modulus reduction and damping curve, with the caveat that the waste not be over damped. These shear modulus reduction curves are presented in Figure 5-3 (a) and damping curves are shown in Figure 5-3 (b) along with the curves of Matasovic and Kavazanjian (1998).

The seismic response predicted by FLAC 7.0 of a vertical column through the center of the landfill using these modulus reduction and damping curves was compared to the response of the same column predicted using SHAKE and the modulus reduction and damping curves of Matasovic and Kavazanjian (1998) to establish the validity of the curves used in FLAC 7.0. Figure 5-4 presents the comparison of the acceleration response spectrum at the top of the vertical column through the center of the waste predicted by FLAC to that predicted by SHAKE. The shear modulus reduction and damping curves used in the analysis illustrated in Figure 5-4 were employed in the two-dimensional FLAC 7.0 seismic analysis or the landfill described in this chapter.

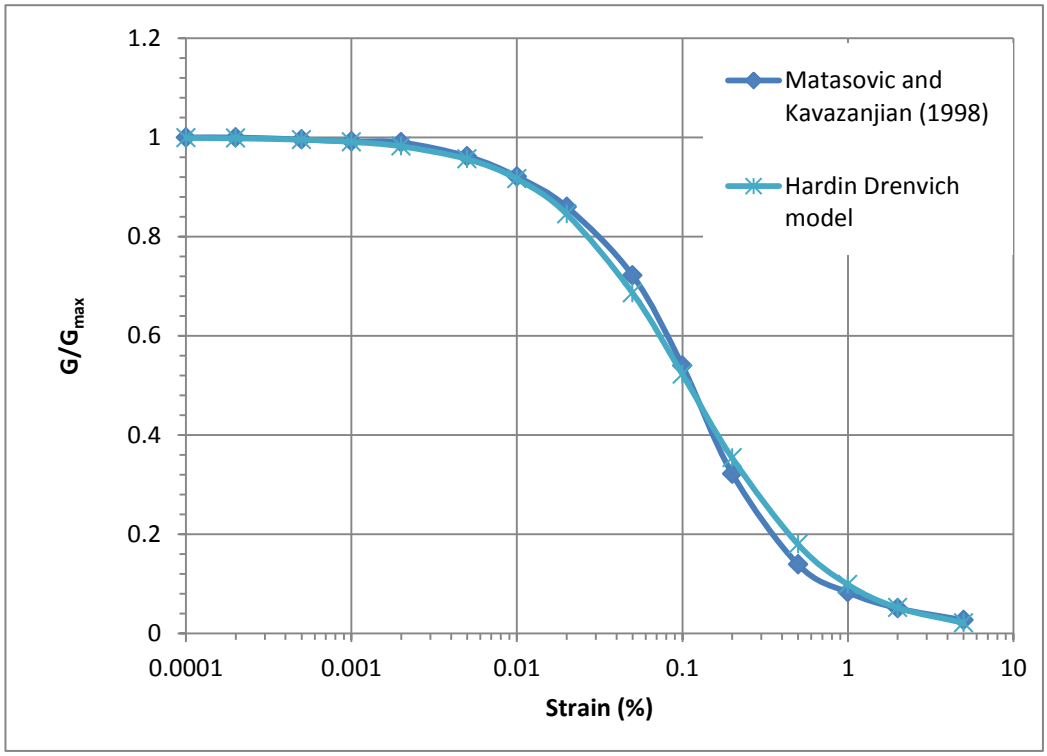

(a)

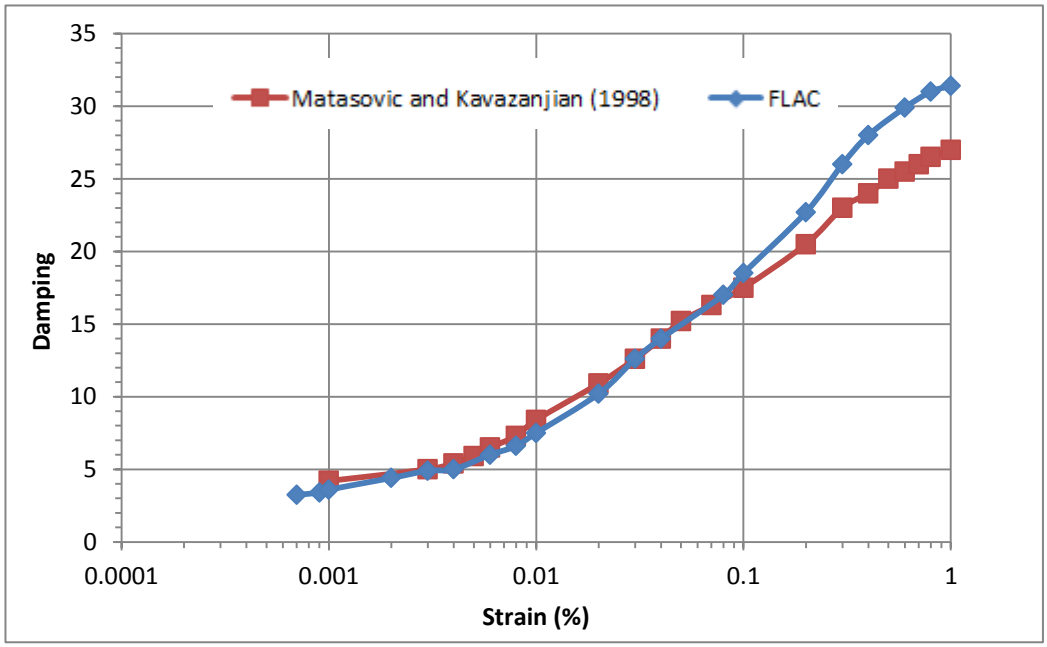

(b)

Figure 5-3 Equivalent linear curves employed in the FLAC 7.0 analyses: (a) modulus reduction; (b) damping curve

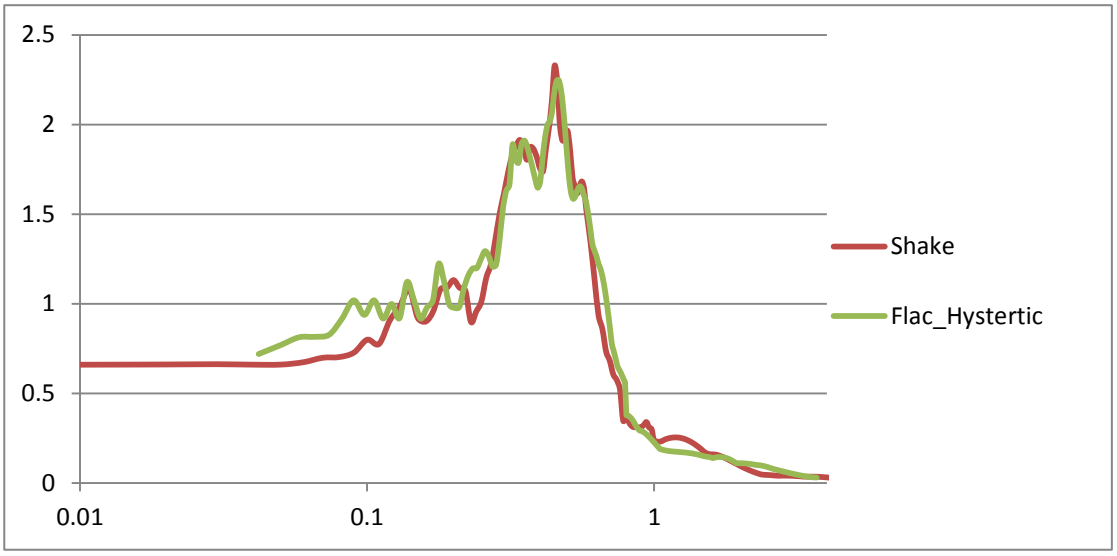

Figure 5-4 Acceleration response spectrum at the top of the vertical column through the center of the waste

5.4 NON-LINEAR 2-D SEISMIC ANALYSES

The finite difference model developed to analyze the seismic response of the landfill cross section is presented in Figure 5-5. The layering in the model was developed such that each layer had approximately the same overburden stress in the middle of the layer and thus the same shear wave velocity and unit weight. In the seismic analysis quiet boundaries were used for the vertical side boundaries and the bottom boundary of the model to absorb the outgoing (downward and outward propagating) seismic waves instead of reflecting them back into the model.

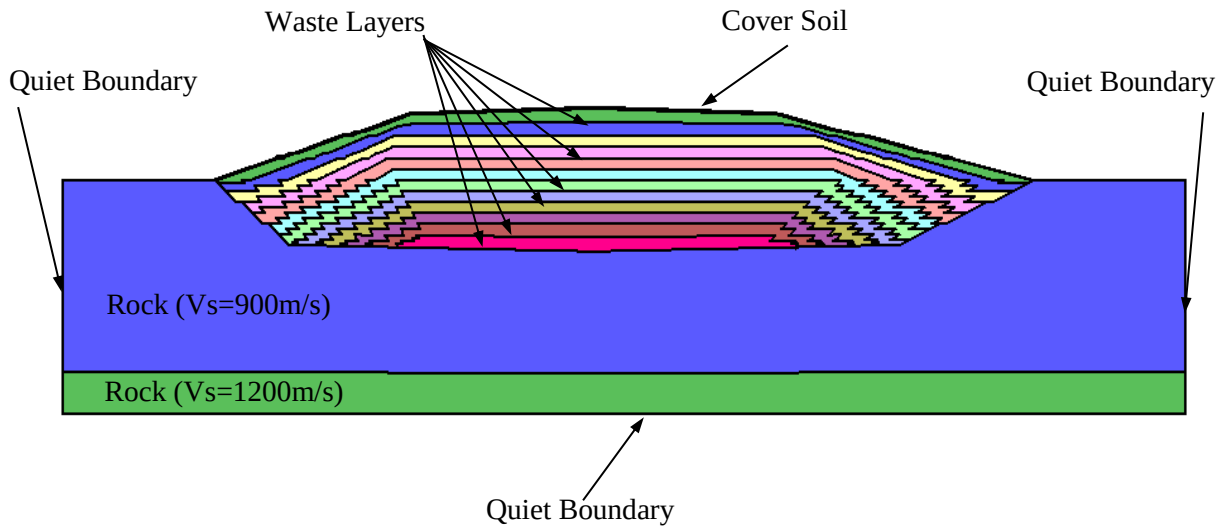

Figure 5-5 Finite difference model with boundary conditions for seismic analyses

5.5 GEOMEMBRANE STRAINS

The seismic analyses were conducted with the cover geomembrane and an overlying final cover soil layer in place. The same three combinations of upper and lower interface strength were used in this analysis as used in the static settlement analyses presented in Chapter 4. These interface strength values are presented in Table 4.2. The strong motion record rotated to an azimuth of 60 degrees from the Pacoima Dam Downstream recording station was used in the analysis. Table 5-2 and 5-3 present a summary of the total maximum tensile strain induced by waste settlement (previous static analysis in Chapter 4) and the additional seismic loading in the geomembrane liner for the 2-D non-linear analyses along with the upper and lower interface shear strength used in the analyses.

The cover system was analyzed by fixing the overlying cover soil to the geomembrane and employing an interface friction angle of 15 degrees to the lower interface. Fixing the cover soil to the geomembrane essentially set the upper interface strength equal to the strength of the cover soil and was assumed to represent a worst case with respect to the strains in the cover system geomembrane. An interface friction angle of 15 degrees was employed as a typical value for the lower interface. Table 5-4 presents the distribution of tensile strains predicted in the geomembrane of cover system.

The reported seismic strains in Tables 5.2 through 5.4 are the combined strains, i.e. the strains due to both static settlement and seismic loading, at the end of earthquake, which is when the maximum tensile strain occurred. The combined maximum axial strains in the liner for the two different slope inclinations in the model (i.e. on the two sides of the model) are presented graphically in Figure 5-6(a), (b) and (c) for the three combinations of upper and lower interface strength considered in the analyses. The combined maximum axial strains in the bottom liner are presented in Figure 5-7 (a), (b) and (c) for the three combinations of upper and lower interface strength considered in the analyses.. The combined maximum axial strains in the cover geomembrane for the one interface strength case considered in the analysis are presented in Figure 5-8.

Table 5-2 Maximum tensile strains in the geomembrane side slope liner after seismic loading

Test Number	Lower Interface Friction Angle ϕ_L (deg)	Upper Interface Friction Angle ϕ_U (deg)	$\Delta\tan\phi = \tan\phi_U - \tan\phi_L$	Tensile Strains (Seismic) (%)	
				1H:1V	2H:1V
1	10 °	20 °	0.188	27.0	7.2
2	16 °	20 °	0.077	12.9	3.3
3	25 °	15.5 °	-0.188	4.1	1.4

Table 5-3 Maximum tensile strains in the geomembrane base liner after seismic loading

Test Number	Lower Interface Friction Angle ϕ_L (deg)	Upper Interface Friction Angle ϕ_U (deg)	$\Delta\tan\phi = \tan\phi_U - \tan\phi_L$	Tensile Strains (Seismic) (%)
				1H:1V
1	10 °	20 °	0.188	2.0
2	16 °	20 °	0.077	1.7
3	25 °	15.5 °	-0.188	0.8

Table 5-4 Maximum tensile strains in the cover geomembrane after seismic loading

Test Number	Lower Interface Friction Angle ϕ (deg)	Maximum Tensile Strains (Seismic) (%)		
		3H:1V	4H:1V	Cover
1	15 °	3.2	1.9	4.3

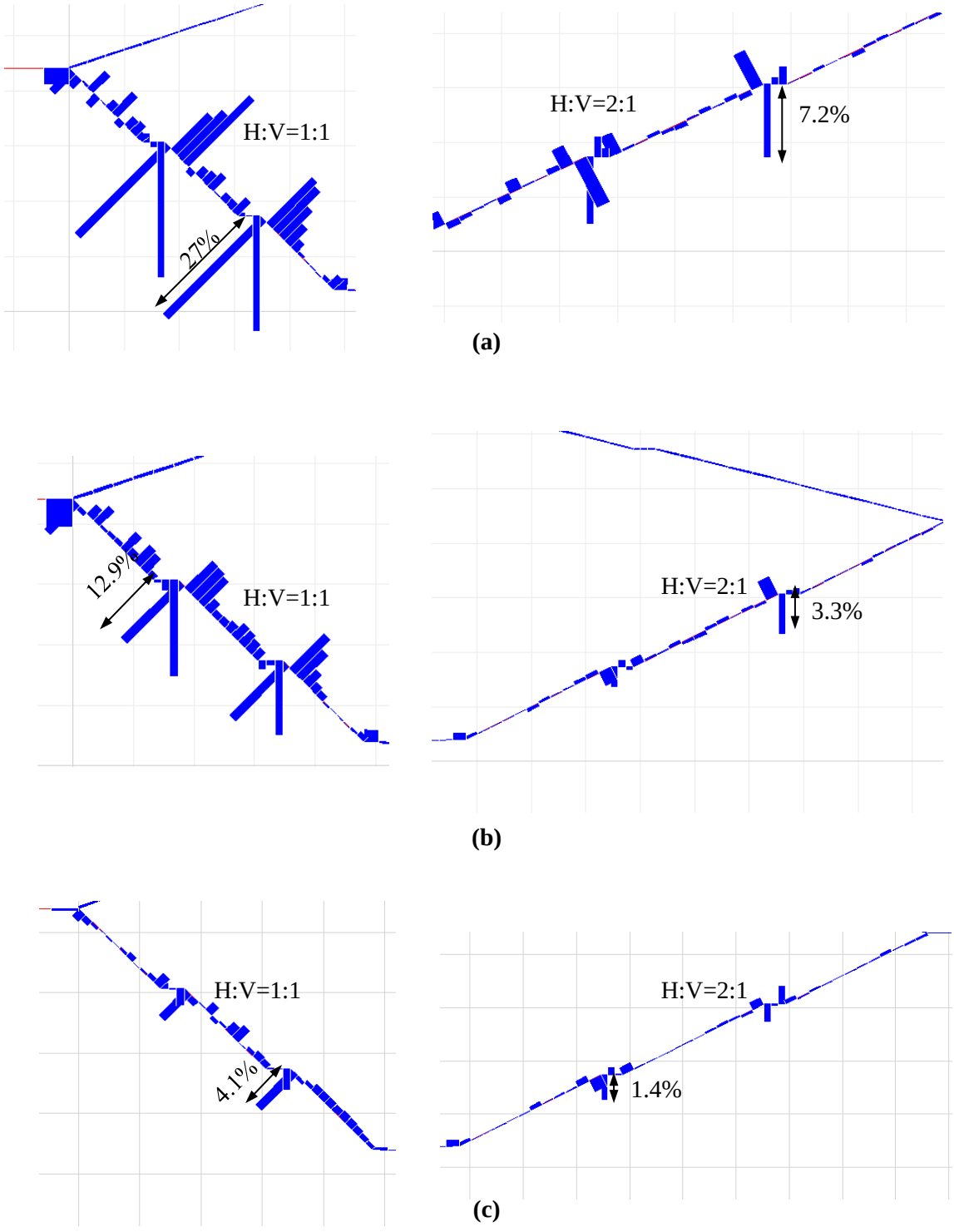

Figure 5-6 The axial tensile strains induced in the side slope geomembrane liner from combined static settlement and seismic loading: a) ϕ_L = 10 °, ϕ_U = 20 °; b) ϕ_L = 16 °, ϕ_U = 20 °; c) ϕ_L = 25 °, ϕ_U = 15.5 °

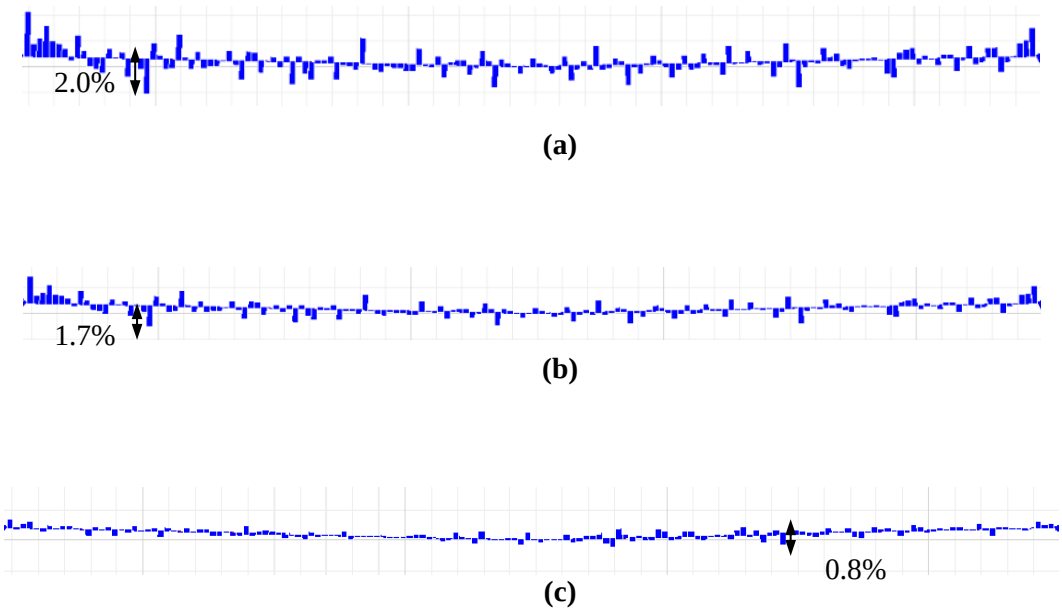

Figure 5-7 The combined axial tensile strains induced in the base liner geomembrane by static settlement and seismic loading: a) ϕ_L = 10 °, ϕ_U = 20 °; b) ϕ_L = 16 °, ϕ_U = 20 °; c) ϕ_L = 25 °, ϕ_U = 15.5 °

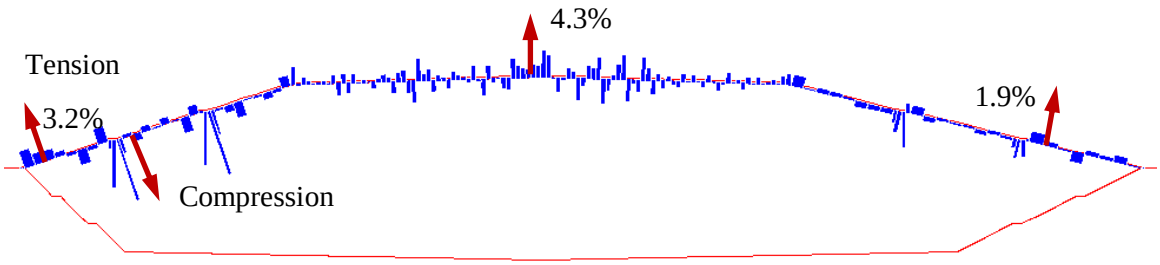

Figure 5-8 The combined axial tensile strains in the cover system geomembrane: ϕ_L = 16 °, ϕ_U = fixed

5.6 SUMMARY FOR SEISMIC ANALYSIS

Two-dimensional non-linear numerical analyses have been conducted of the seismic response of the landfill model developed in the previous chapter using FLAC 7.0 and the Pacoima Dam Downstream input motion of the Northridge earthquake. The Pacoima Dam Downstream input motion rotated to a 60 degree azimuth, with a 0.49 g PGA, was employed in the analysis reported herein. To transform this bedrock outcrop strong motion record into a subsurface ground motion that can be applied at the base of the 2-D FLAC 7.0 model used in this analysis a deconvolution procedure using the computer program SHAKE was employed. The unit weight of the waste and shear wave velocity used in the analysis were based on the previous analysis of waste placement and static settlement presented in Chapter 4. The shear modulus reduction and damping curves used in FLAC analysis were developed based upon curves for MSW recommended by Matasovic and Kavazanjian (1998) developed from back analysis of the seismic response of the Operating Industries, Inc. landfill in southern California.

The seismic analyses were conducted using beam elements with zero moment of inertia to model the geomembrane. The beam elements were fitted with interface elements that allow for slip at the interface on both sides of the geomembranes. The seismic loading was induced on top of the strains imposed in the geomembrane by static

settlement due to both waste placement and post-placement waste decomposition. The seismic motion induced additional strains in both liner and cover system geomembranes.

The reported seismic strains are the combined strains at the end of earthquake, which was when the maximum tensile strain occurred. The results are consistent with the results from the static settlement analysis in that the axial strains and forces in the geomembranes are dependent upon the slope inclination and the upper and lower interface shear strengths (friction angles). The combined tensile strain in side slope geomembrane due to settlement and seismic loading still was the least for the case where $\phi_U < \phi_L$, i.e. for $\phi_U = 15.5°$ and $\phi_L = 25°$, with a maximum tensle strain of 4.1% for the 1H:1V slope and 1.4% for the 2H:1V slope. Tension in the geomembrane was greater for the two cases of $\phi_U > \phi_L$ with maximum tensile strains of 7.2% in 1H:1V and 3.3% in 2H:1V for the case of $\phi_L = 16°$, $\phi_U = 20°$, (the lower value of $\Delta\tan\phi$) and a maximum tensile strain of 27% in 1H:1V slope and 2.9% in 2H:1V slope for $\phi_U = 20°$ and $\phi_L = 10°$ (the higher $\Delta\tan\phi$ value used in the analysis).

For the bottom geomembrane liner, there were no significant tensile strains in any of the three cases of analysis. The maximum tensile strain was no more than 2% after seismic loading in any case. The tensile strain in cover system was also small in all cases. For the 3H:1V slope, the maximum tensile strain in the cover system was 3.2%, and the maximum tensile strain was 1.9% for 4H:1V slope. There was also a tensile strain of 4.3% induced in the cover system geomembrane on top deck by seismic loading.

CHAPTER 6 SUMMARY AND CONCLUSIONS

6.1 SUMMARY

To develop guidelines for identifying when settlement or seismic loading presents a threat to the integrity of geomembrane barrier layers for both side slope and cover systems in landfills, a numerical model of a typical canyon landfill with different side slope inclinations was developed using the two-dimensional explicit finite difference program FLAC 7.0. Beam elements with a hyperbolic stress-strain relationship, zero moment of inertia, and interface elements with frictional shear resistance on both sides were used to model the geomembranes. The interface shear parameters of the geomembranes and inclinations of the landfill side slope and cover were varied to develop an understanding of how these parameters influence the tensile forces and strains in the liner and cover system geomembranes.

The engineering characteristics of the various components of landfill (e.g. solid waste, geosynthetic lining material) were verified in modeling. Landfill settlement during waste placement and post-placement was modeled using the Modified Cam-Clay (MCC) constitutive model for the waste. The MCC parameters employed during waste placement were based on the results of oedometer tests conducted by GeoSyntec (1995) on OII landfill solid waste material. To model the post-placement waste settlement, the slope of virgin consolidation line λ was adjusted after the conclusion of waste placement until the change induced a settlement approximately equal to 20% of the waste thickness

at the end of waste placement (a value chosen as typical of the amount of post-closure landfill settlement). The unit weight of waste and shear velocity versus depth was calculated following the induced post-placement settlement and were shown to be consistent with reported values for these properties.

In the seismic analysis, the waste was modeled using the equivalent liner material model. The shear modulus reduction and damping curves for the waste were based upon the MSW shear modulus reduction and damping curves recommended by Matasovic and Kavazanjian (1998). Initial values for the parameters describing the shear modulus reduction and damping curves were adjusted until the seismic response for a column through the center of the landfill predicted using these parameters and FLAC 7.0 was essentially the same as that predicted using the shear modulus reduction and damping curves proposed by Matasovic and Kavaznjian (1998) and the computer program SHAKE.

The in-plane stress-strain behavior of the interface elements was modeled as a linear elastic-perfectly plastic Mohr-Coulomb material. The initial stiffness and elastic modulus for the geomembrane interfaces were based upon the numerical analysis for Chiquita Canyon landfill by Arab (2011). Three different sets of upper and lower interface shear strengths were employed in the numerical analysis to evaluate the impact of these parameters on geomembrane forces and strains.

The geometry used in the numerical model employed in this research was based upon typical side slope liner geometry for steep-sided canyon landfills in California, e.g. Disposal Area C of the City of Los Angeles Lopez Canyon landfill and Canyons C and D at the Chiquita Canyon landfill (Arab 2011). Multiple side slope angels were modeled in the analysis: 1H:1V and 2H:1V slopes were modeled for the side slope liner; 3H:1V and 4H:1V slopes were modeled for the cover system). Both side slope liner and cover included horizontal benches at 12 m (40 ft) vertical intervals. For the seismic analysis, the strong motion record from the Pacoima Dam Downstream recording station in the Northridge earthquake rotated to an azimuth of 60 degrees (0.49 PGA) was used.

6.2 CONCLUSIONS FOR RESULTS

The results of both the static and seismic analyses indicate that the axial strains and forces in both the liner and cover systems are sensitive to the slope inclination and the values of the upper and lower geomembrane interface shear strength (friction angle). The tension in geomembrane is least when the upper interface friction angle was lower than the lower interface friction angel, but could still be of engineering significance following post-closure settlement and seismic loading even if this was the case.

Tension in the geomembrane for the case of $\phi_U > \phi_L$ depended upon both the value of $\Delta\tan\phi$ and the absolute values of ϕ. The higher the value of $\Delta\tan\phi$ between interfaces on the top and bottom of th geomembrane the greater the axial tensile strain induced in geomembrane. The side slope inclination also influences the value of tensile strain

induced in the geomembrane. The results show that the maximum tension in geomembrane is greater in the steeper slopes and always occurs at the top of a slope segment just below the bench or on the bench itself.. In the two cases for which $\phi_U > \phi_L$, the combined tensile strains in the geomembrane for the 1H:1V slope were greater than 12% after seismic loading, which is clearly not acceptable for HDPE geomembrane. For the 2H:1V slope, the maximum combined tensile strain was 7.2% for the case where $\phi_L = 10°$ and $\phi_U = 20°$, an unacceptable value, but reduced to 3.3% for $\phi_L = 16°$ and $\phi_U = 20°$, a marginal but possibly acceptable value (depending upon the location of horizontal seams in the geomembrane). For the case where $\phi_U < \phi_L$, the steeper side slope (i.e. the 1H:1V slope) the induced tensile strain due to combined settlement and seismic loading was 4.1%, which is marginal in terms of the allowable tensile strain in a HDPE liner. However, the maximum tensile strain in the 2H:1V slope were 1.4%, a are much lower value which is generally acceptable. Tensile strains induced in the base geomembrane due to combined waste settlement and seismic loading were small for all cases investigated in this research.

Tensile strains due to post-placement waste settlement in the cover system geomembrane are very low for both side slope inclinations investigated 9i.e. 3H:1V and 4H:1V). After seismic loading, of the tensile strains in te cover system increased, reaching a maximum value of 4.3% on the top deck. While this value is marginally acceptable for HDPE geomembranes, cover system geomembranes are genrally

composed of more ductile Low Density Polyethylene (LDPE) which has a greater allowable strain. Furthermore, damage to a cover system geomembrane is detectable and can be repaired. Therefore, this level of tensile strain is considered to be acceptable for a cover system geomembrane.

An important finding from this study is that tension is greatest in a geomembrane at the top of a slope segment or on the benches. This suggests that horizontal geomembrane seams, i.e. seams parallel to the slope contour wherein strain concentrations signifcnatly reduce the allowable tensile strain, should be avoided if at all possible in these areas. Most geosynthetic specifications do not allow continuous seams parallel to the slope contour on landfill side slopes. However, seams parallel to the slope contour will occur at locations where samples of the seam are recovered for destructive testing in the laboratory. Therefore, it would seem prudent that construction quality assurance guidelines prohibit recovery of samples for destructive laboratory testing from benches and within 2 m (6 ft) of the top of the slope, i.e. in the areas where the largest tensile strains are likely to develop).

REFERENCES

Mohamed, A. (2011). The Integrity of Geosynthetic Elements of Waste Containment Barrier Systems Subject to Seismic Loading. A Dissertation Presented in Partial Fulfillment of the Requirements for the Degree Doctor of Philosophy, Arizona State University, Tempe, Arizona

AASHTO (2007). AASHTO LRFD Bridge Design Specifications. 4th Edition, American Association of State Highway and Transportation Officials.

Anderson, D. G., and Kavazanjian, E., Jr. (1995) Performance of Landfills Under Seismic Loading. Proc. 3rd International Conference on Recent Advances in Geotechnical Earthquake Engineering and Soil Dynamics, University of Missouri-Rolla, Rolla, Missouri, Vol. III, pp. 1-30.

Anderson, D. G., Martin, G. R., Lam, I., and Wang, J. N. (2009). Seismic analysis and design of retaining walls, buried structures. slopes, and embankments. NCHRP Rep. 611, Transportation Research Board, Washington, D.C.

Fowmes, G.J. (2007). Analysis of Steep sided Landfill Lining System. Eng.D thesis, Department of Civil and Building Engineering, Loughborough University, Loughborough, UK.

Kavazanjian, E., Jr., Dixon, N., Katusmi, Y., Kortegast, A., Legg, P., and Zanzinger, H. (2006). Geosynthetic Barriers for Environmental Protection at Landfills. Proceedings, 8th International Conference on Geosynthetics, J. Kuwano and J. Koseki, eds., Yokohama, Japan, 121-152.

Kavazanjian, E., Jr., Hushmand, B., and Martin, G.R. (1991). Frictional Base Isolation Using a Layered Soil-Synthetic Liner System, Proceedings, 3rd U.S. Conference on Lifeline Earthquake Engineering, ASCE Technical Council on Lifeline Earthquake Engineering Monograph Vol. 4:1139-1151.

Kavazanjian, E., Jr., Matasovic, N. Bonaparte, R. and Schmertmann, G.R. (1995), Evaluation of MSW Properties for Seismic Analysis, In: Geoenvironment 2000, ASCE Geotechnical Special Publication No. 46, Vol. 2, pp. 1126-1141.

Kavazanjian, E., Jr., Matasovic, N., and Caldwell, J.A. (1998). Seismic Design and Performance Criteria for Landfills, Proceedings, 6th US National Conference on Earthquake Engineering, Seattle, Washington (CD-ROM).

Kavazanjian, E., Jr., Matasovic, N., Stokoe, K.H., II, and Bray, J.D. (1996). In-Situ Shear Wave Velocity of Solid Waste from Surface Wave Measurements, Proc. 2nd International Congress Environmental Geotechnics, Osaka, Ja98pan, Balkema, Vol. 1, pp. 97-104

Fox, P. J., and Stark, T. D. (2004). State-of-the-art report: GCL shear strength and its measurement, Geosynthetics International, 11(3), 141-175.

Fox, P.J., and Kim, R.H. (2008). Effect of progressive failure on measured shear strength of geomembrane/GCL interface. Journal of Geotechnical and Geoenvironmental Engineering, 134(4): 459-469.

Giroud, J. P. (1984). Analysis of stresses and elongations in geomembranes. Proceedings of the International Conference on Geomembranes, Denver, CO, IFAI Publisher, Vol. 2, pp. 481–486.

Giroud, J. P. (1993). Lessons learned from studying the performance of geosynthetics. Proceedings of Geotextiles-Geomembranes Rencontres 93, Joue ́-les-Tours, France, CFG Publisher, Vol. 1, No. 15, pp. 33–46.

Giroud, J. P. (2005). Quantification of geosynthetic behavior. *Geosynthetics International*, Special Issue on the Giroud Lectures, 12, No. 1, 2-27.

Idriss, I.M., Fiegel, G., Hudson, M.B., Mundy, P.K., and Herzig, R. (1995). Seismic response of the Operating Industries landfill. Earthquake design and performance of solid waste landfills, ASCE Geotechnical Special Publication No. 54, *Edited by* M.Y. Yegian, W.D. Liam Finn, 83-118.

Itasca (2008) FLAC version 600 user's guide – Fast Lagrangian analysis of continua, user' s manual Itasca Consulting Group, Inc., Minneapolis, MN

Matasovic, N. (2010). D-MOD2000 - A Computer Program for Seismic Response Analysis of Horizontally Layered Soil Deposits, Earthfill Dams, and Solid Waste Landfills, User ' s Manual, GeoMotions, LLC (www.GeoMotions.com), Lacey, Washington.

Zekkos, J.D. Bray, J.E. Kavazanjian, N. Matasovic, E.M. Rathje, M.F. Riemer and K.H. Stokoe, (2006). Unit weight of municipal solid waste. *Journal of Geotechnical and Geoenvironmental Engineering*, 132, No. 10, 1250-1261.